A facultative ectomycorrhizal association is triggered by organic nitrogen

Long Peng, Yan Zhang, Irina Druzhinina, Christian Kubicek, Yuchen Wang, Zhiyong Zhu, Yuwei Zhang, Kexuan Wang, Zhuo Liu, Xiaoguo Zhang, et al.

Article

Current Biology

A facultative ectomycorrhizal association is triggered by organic nitrogen

Graphical abstract

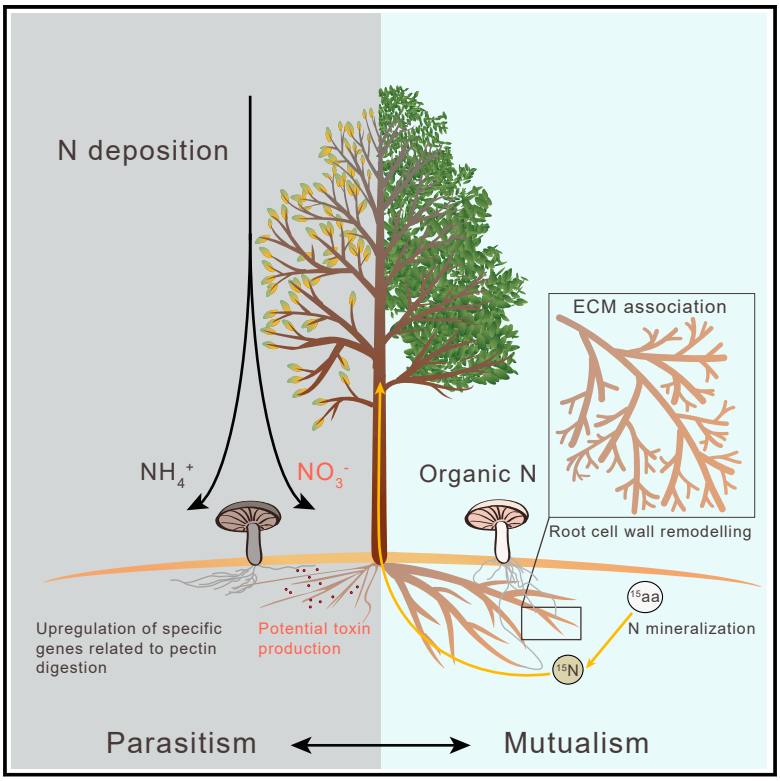

Highlights

- Ammonium dampens mutualism by upregulating specific genes related to pectin digestion
- Nitrate impairs mycorrhizae by inducing toxin synthesis by the fungus
- Organic nitrogen favors mutualistic ectomycorrhizal interactions
- *C. hobsonii* is a facultative mycorrhizal fungus capable of parasitism and saprotrophy

Authors

Long Peng, Yan Zhang, Irina S. Druzhinina, ..., Xiaoguo Zhang, Francis Martin, Zhilin Yuan

Correspondence

francis.martin@inrae.fr (F.M.), yuanzl@caf.ac.cn (Z.Y.)

In brief

Peng et al. show that soil nitrogen influences the mode of nutrition in tree-fungal interactions. Organic nitrogen favors mutualistic mycorrhizal association, whereas mineral nitrogen leads to a detrimental effect of the fungus on plant. This work reveals the remarkable physiological remodeling of fungi in response to their environment.

Peng et al., 2022, Current Biology *32*, 5235–5249
December 19, 2022
https://doi.org/10.1016/j.cub.2022.10.054

CellPress

Current Biology

CellPress

Article

A facultative ectomycorrhizal association is triggered by organic nitrogen

Long Peng,[1,2] Yan Zhang,[3] Irina S. Druzhinina,[4] Christian P. Kubicek,[5] Yuchen Wang,[1,2] Zhiyong Zhu,[2] Yuwei Zhang,[1,2] Kexuan Wang,[1,2] Zhuo Liu,[1,2] Xiaoguo Zhang,[2] Francis Martin,[6,*] and Zhilin Yuan[1,2,7,*]

[1]State Key Laboratory of Tree Genetics and Breeding, Chinese Academy of Forestry, Dongxiaofu 1, Beijing 10091, China
[2]Research Institute of Subtropical Forestry, Chinese Academy of Forestry, Daqiao Road 73, Hangzhou 311400, China
[3]Liaoning Provincial Institute of Poplar, Gaizhou 115213, China
[4]Royal Botanic Gardens, Kew, Richmond TW9 3AE, UK
[5]Institute of Chemical, Environmental & Bioscience Engineering (ICEBE), TU Wien, Vienna A1060, Austria
[6]Université de Lorraine, INRAE, UMR 1136 "Interactions Arbres/Microorganismes," Centre INRAE Grand Est - Nancy, Champenoux 54280, France
[7]Lead contact
*Correspondence: francis.martin@inrae.fr (F. M.), yuanzl@caf.ac.cn (Z. Y.)
https://doi.org/10.1016/j.cub.2022.10.054

SUMMARY

Increasing nitrogen (N) deposition often tends to negatively impact the functions of belowground ectomycorrhizal networks, although the exact molecular mechanisms underlying this trait are still unclear. Here, we assess how the root-associated fungus *Clitopilus hobsonii* establishes an ectomycorrhiza-like association with its host tree *Populus tomentosa* and how this interaction is favored by organic N over mineral N. The establishment of a functional symbiosis in the presence of organic N promotes plant growth and the transfer of ^{15}N from the fungus to above ground plant tissues. Genomic traits and *in planta* transcriptional signatures suggest that *C. hobsonii* may have a dual lifestyle with saprotrophic and mutualistic traits. For example, several genes involved in the digestion of cellulose and hemicellulose are highly expressed during the interaction, whereas the expression of multiple copies of pectin-digesting genes is tightly controlled. Conversely, the nutritional mutualism is dampened in the presence of ammonium (NH_4^+) or nitrate (NO_3^-). Increasing levels of NH_4^+ led to a higher expression of pectin-digesting genes and a continuous increase in hydrogen peroxide production in roots, whereas the presence of NO_3^- resulted in toxin production. In summary, our results suggest that *C. hobsonii* is a facultative ectomycorrhizal fungus. Access to various forms of N acts as an on/off switch for mutualism caused by large-scale fungal physiological remodeling. Furthermore, the abundance of pectin-degrading enzymes with distinct expression patterns during functional divergence after exposure to NH_4^+ or organic N is likely to be central to the transition from parasitism to mutualism.

INTRODUCTION

Plant-microbe interactions are profoundly affected by environmental conditions.[1,2] For example, exposure to bright light triggers pathogenic behavior by the fungus *Diplodia mutila* (Botryosphaeriales, Ascomycota), whereas reduced illumination favors endophytic development.[3] The impact of nutrient levels on symbiotic behavior is also recognized.[4–7] High levels of nitrogen (N) and phosphorus (P) often prevent establishing mutualistic interactions, as manifested in N-fixing rhizobia, arbuscular mycorrhizal (AM), and endophytic fungi. The molecular mechanisms linking nutrient levels to symbiosis are investigated in detail during N-fixing in leguminous plants.[8] Legumes use two signaling peptides, the C-terminally encoded peptides and the CLAVATA3/endosperm surrounding region-related peptides, to inversely regulate nodulation.[9] The expression of these genes is under the control of the nodule inception transcription factor, allowing the plant to sense, and appropriately respond to, changing levels of N.[10] The recent discovery of a P-sensing pathway regulated by a network of phosphate starvation response transcription factors in AM symbiosis[11] suggests that symbiotic plants are evolved robust and conserved mechanisms to respond to changing nutrient levels.[12]

A less investigated, but equally important, question is how symbiotic microbes sense soil nutrient forms available to them. Globally, the ongoing deposition of high levels of anthropogenic N, primarily in mineral form, poses a major ecological threat. This raises an intriguing question about how the unbalanced N cycle, the changing ratio of organic and mineral N, and the resulting ecological consequences impact on biotic interactions, such as plant-microbe symbiosis. Large-scale ecological observations suggest that the disruption of belowground ectomycorrhizal (ECM) networks and the increase of tree pathogen diversity correlate closely with increasing N deposition.[13–18] However, the mechanisms underlying the mycorrhizal dysfunction remain poorly explained.

Filamentous fungi are known to exhibit divergent physiological behaviors when utilizing different N forms. Most ECM fungi

preferentially utilize organic N, such as amino acids, followed by ammonium (NH_4^+),[19–21] whereas only a small proportion of taxa appear to readily metabolize nitrate (NO_3^-) as sole N source.[13,22] These foraging preferences presumably correlate with the N status of their soil habitats.[23,24] It is tempting to speculate that changes in available N forms could lead to a reprogramming of fungal metabolism and then alter the beneficial interactions with hosts. Gallart et al.[25] found that organic N favored the growth of ECM and endophytic fungi, whereas mineral N stimulated the proliferation of saprotrophic/parasitic fungi in soils, ultimately causing disease symptoms in plants[16,26] and reducing Hartig net depth.[15] It is found that different N forms drastically change the physiological status of the versatile basidiomycetous mutualistic endophyte *Serendipita indica*. In this relationship, mineral N supply change the interaction between the plant and *S. indica*, shifting it from mutualistic to antagonistic.[27] With regard to root dark septate endophytes (DSEs), organic N supply is more likely to be beneficial for plant-DSEs associations.[28,29] In the case of alga-protozoan symbiotic association, organic N rather than mineral N stabilizes cooperation within the holobiont.[30] These pieces of evidence raise the question of how different N forms affect the fate of plant-fungus symbiotic associations.

In the present study, we tackled this question by focusing on a novel tree-fungus association involving *Clitopilus hobsonii* (Entolomataceae, Agaricales). This species is considered a soil decomposer because it is widely found in debris of herbaceous or woody plants.[31,32] Also, in our previous studies, *C. hobsonii* could be identified from ECM root tips of oak tree species (*Quercus* spp.).[33,34] Of note, we did not have direct evidence for supporting it as an ECM fungus associated with *Quercus*. Therefore, we remain cautious to consider it a root endophyte, characterized by its ability to promote tree growth and nutrient uptake, especially under low K^+ conditions.[33,35] To investigate how this beneficial association responds to different forms of N, we addressed the following questions: (1) How does the fungus respond to different N forms at the physiological and molecular levels? (2) How do different N forms influence the plant-*C. hobsonii* interaction? (3) What are the main genetic processes contributing to the outcome of this dynamic interaction? (4) Does *C. hobsonii* share genomic idiosyncrasies (e.g., a restricted set of plant cell-wall degrading enzymes [PCWDEs]) with ECM fungal genomes?

RESULTS

C. hobsonii preferentially forages organic N

We measured the *in vitro* N requirements of *C. hobsonii* by growing the fungus on three N sources. Using NO_3^- as an N source, the mycelium produced sparse colonies, with only a thin layer of aerial mycelium, indicating a very poor ability to utilize this N source. This treatment accelerated hyphal growth (12 days, ANOVA, $F = 94.596$, df = 26, $p < 0.001$) (Figures S1A and S1B). In contrast, *C. hobsonii* grew well on NH_4^+ and organic N, with colonies growing on the latter being clearly distinguishable by their larger diameter. Mycelia produced the largest biomass on a liquid medium containing organic N (30 days, ANOVA, $F = 180.69$, df = 14, $p < 0.001$) (Figure S1C), exhibiting a clear preference toward organic N over NH_4^+ and NO_3^-. The different N forms had differential quantitative effects on the growth and morphology of mycelium. It is also noted that NH_4^+ uptake led to a rapid drop of pH, from 5.8 to 2.8, suggesting that the fungus released H^+ into the medium (Figure S1D). The pH values remained unchanged on NO_3^- or increased slightly in the presence of organic N. In addition, the three N forms also changed the ability of the mycelium to penetrate through a cellophane membrane. Penetration was more pronounced on organic N medium (Figure S1E).

C. hobsonii forms a mutualistic interaction with plants if organic N is available, whereas mineral N sources trigger parasitism

When poplar cuttings were grown on NH_4^+- or NO_3^--containing media, shoot growth was considerably reduced in the presence of *C. hobsonii*, and the development of newly grown roots was completely arrested with wilting and falling leaves. Under these conditions, fungal hyphae even extended to aboveground plant tissues including stems and leaves. After a prolonged exposure to the mycelium, signs of shoot necrosis appeared (Figures 1A and S2A), indicating aggressive fungal colonization. In contrast, no conspicuous disease development was observed when the plants and the fungus were cultured in the presence of organic N, and hyphae growing outside the inoculated roots did not extend to the aboveground tissues (Figure 1A). Furthermore, numerous adventitious roots were produced after 2 weeks of incubation. This beneficial interaction appeared to be stable over months of co-cultivation (Figure S2B). Initially, a mixture of five amino acids was used as an organic N source, whereas in later experiments, we confirmed the beneficial effect of organic N by using bovine serum albumin (BSA) (Figure S2C). Taken together, these findings suggest that *C. hobsonii* behaves as a beneficial biotrophic fungus in the presence of organic N, whereas acting as a pathogen when fed on mineral N. Notably, WGA staining confirmed that *C. hobsonii* developed intercellular hyphae resembling the Hartig net and mycorrhizal mantle-like structures inside the roots 1 month post-inoculation (Figures 1B and 1C). Furthermore, non-ECM roots were heavily colonized by microsclerotia-like structures consisting of aggregates of spherical hyphal cells (Figure S3). These, in most cases, filled entire root cells, reminiscent of DSE interactions. This colonization pattern was analogous to that observed in the symbiotic system between sweetgum tree and *C. hobsonii*.[35]

Based on the observed phenotypic alterations of inoculated plants, we speculated that the fungus was parasitic when grown on mineral N. H_2O_2 generation from the oxidative burst is a common plant immune response in both pathogenic and beneficial plant-fungus interactions.[36] Thus, H_2O_2 abundance was measured and compared in roots under the three N form-plant-fungus combinations, across two time points. Histological imaging showed the most prominent dark brownish-red precipitate staining in root tips after 12 h post-inoculation in the presence of NH_4^+. Under organic N condition, H_2O_2 production was less pronounced but still evident (Figure 1D). In contrast, almost no H_2O_2 generation was observed in NO_3^- (Figure 1D) (ANOVA, $F = 43.372$, df = 92, $p < 0.001$). 60 h post-inoculation, root H_2O_2 contents increased significantly in the presence of NO_3^-, whereas a reduction was seen under organic N condition (ANOVA, $F = 42.364$, df = 96, $p < 0.001$). The accumulation of

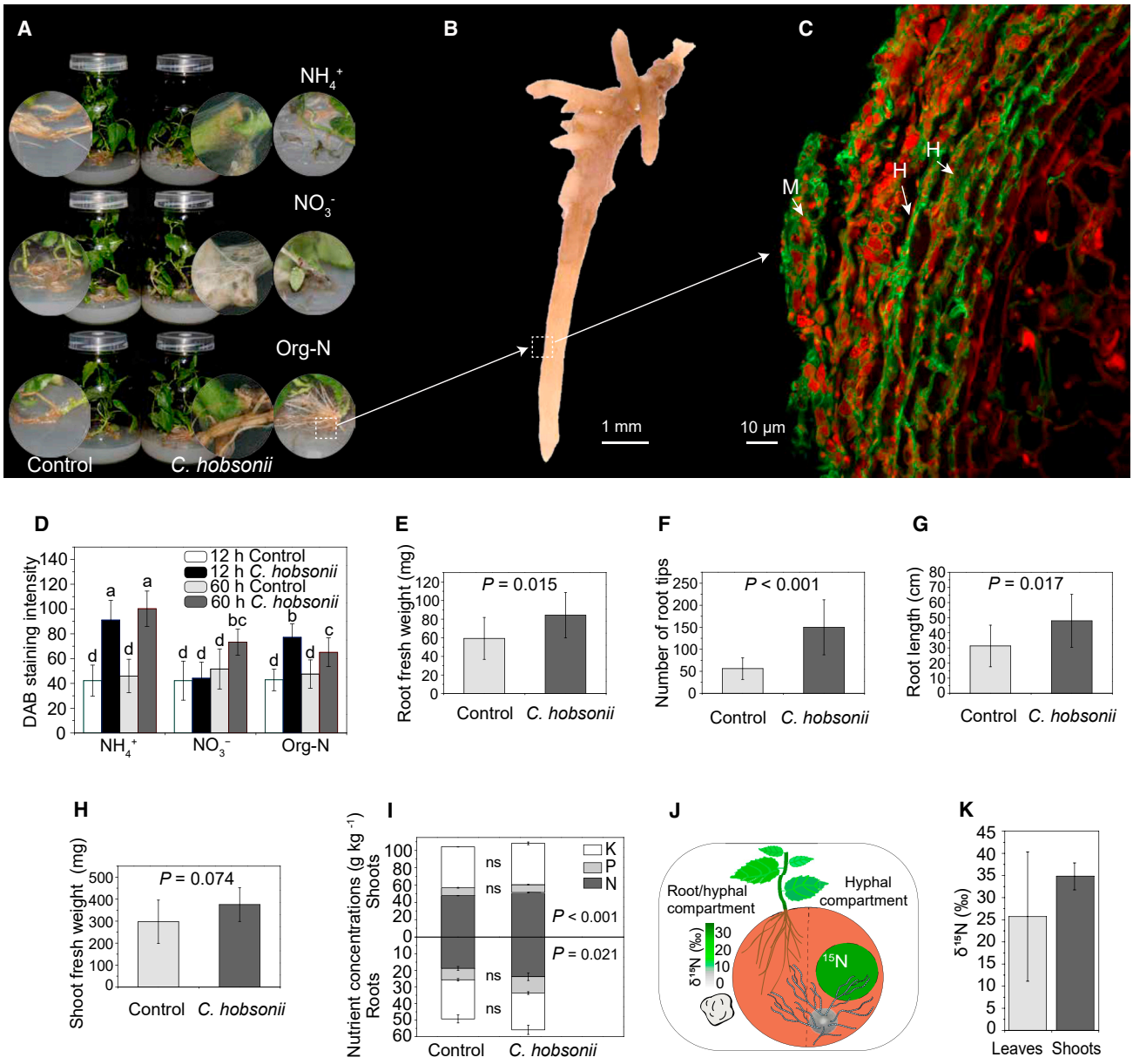

Figure 1. Organic N triggers ectomycorrhizal development in plant-*C. hobsonii* association

(A) Impact of three N forms on the outcomes of plant-*C. hobsonii* interactions. Under organic N condition, the fungus benefits poplar growth, improving adventitious rooting. Plant growth is severely inhibited upon inoculation under mineral N (either NH_4^+ or NO_3^-) conditions, and mycelia are extended to aboveground plant tissues. Plants are photographed at 4 weeks after incubation.

(B) Ectomycorrhizal-like root development, photographed by an ultra-depth-of-field optical microscope.

(C) Transverse section of ectomycorrhizal root tips. Plant cell walls are stained with PI and fungal hyphae are labeled with WGA. Mantle-like structures, and Hartig nets are indicated by white arrows. M, mantle; H, Hartig net.

(D) Quantification of DAB staining intensity at 12 and 60 h after root inoculation, showing contrasting H_2O_2 production under the three N forms conditions. At least 12 root tips from each treatment group are inspected for greater accuracy. Statistical significance is calculated using ANOVA ($p < 0.05$). Error bars represent SD of replicates. Different lowercase letters indicate significant differences.

(E–H) In each comparison, 12 plants per treatment are used to measure plant phenotype, including root fresh weight (E), number of root tips (F), root length (G), and shoot fresh weight (H) at 40 days after incubation. Statistical significance between inoculated and control groups is calculated using Student's two-sample t test.

(I) Measurement of nutrient concentrations (N, P, and K) of belowground and aboveground tissues.

(J) Setup of microcosms for testing N transfer from the mycelia to plant roots. A fungal plug is placed on one side of a split Petri dish containing the organic N medium and grown for 1 week before gnotobiotic plants are placed into the system. A sterile, moistened cotton wool ball is added to protect the plant from drying out. ^{15}N tracer is added to a round chamber in the hyphal compartment.

(K) $\delta^{15}N$ signature detection from the shoots and leaves of plants, indicating active N transfer from *C. hobsonii* to plants. Error bars represent SD of replicates. See also Figure S2.

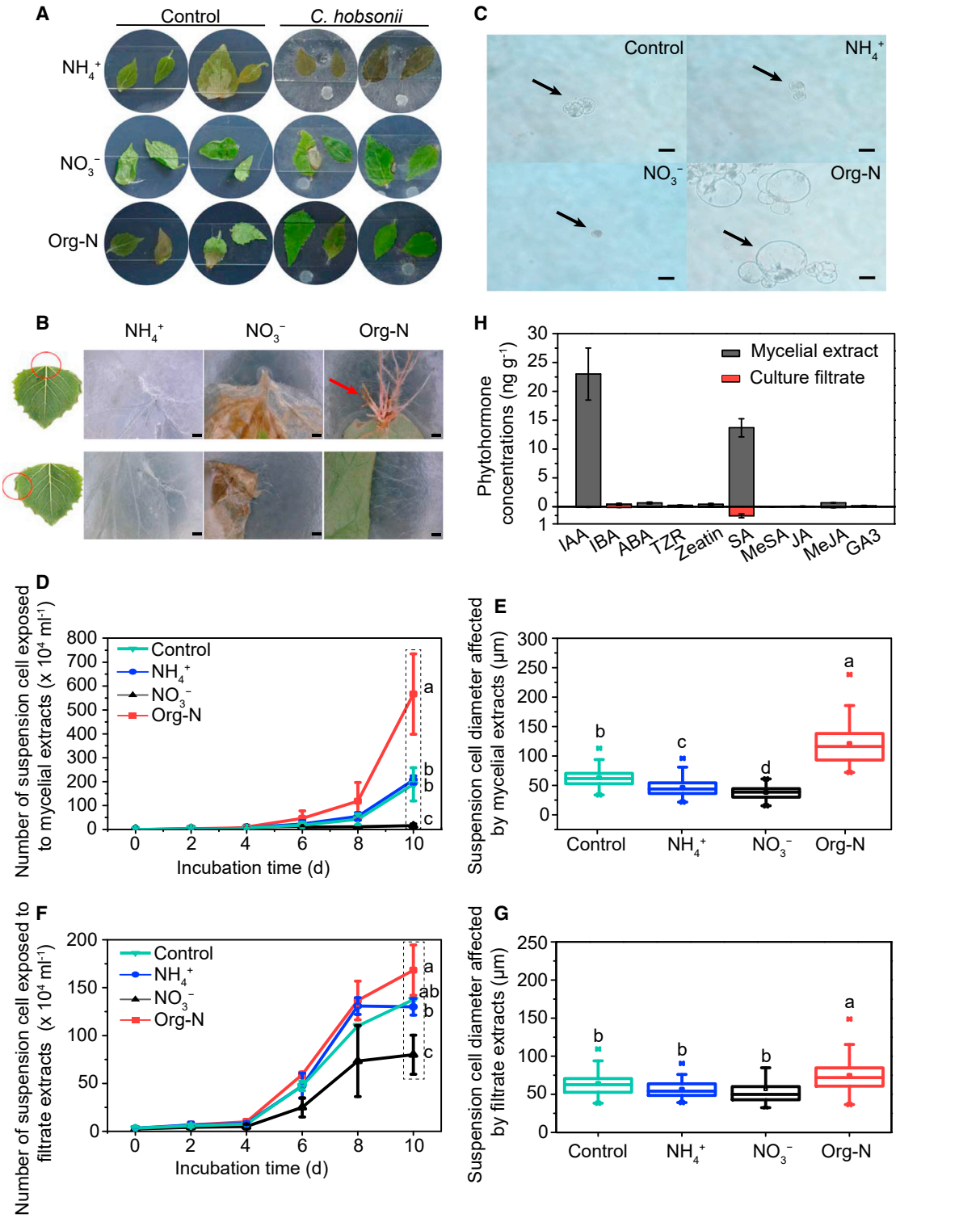

Figure 2. Organic N-fed *C. hobsonii* triggers adventitious rooting in detached leaves and promotes growth in cell suspensions

(A) Mycelia pre-grown on NH_4^+ or NO_3^- induced leaf bleaching and dark-brown lesions, respectively, whereas leaves show no symptoms under organic N condition. Leaves of similar size and age are covered with sterile glass slides to guarantee tight contact. Cultures are maintained at 24°C under a 12 h light/12 h dark cycle in a growth chamber. After 1 week incubation, leaves are photographed.

(B) Organic N-fed mycelia trigger adventitious rooting from the cut end of petioles. Leaves are recorded by an ultra-depth-of-field optical microscope after 4 weeks of inoculation. Newly emerging roots are indicated by a red arrow.

(C) Effects of crude extracts from mycelia fed on three N forms on the growth of poplar suspension cells. Poplar suspension cells are indicated by black arrows.

(legend continued on next page)

H_2O_2 was continuous under NH_4^+ condition (Figure 1D). It is thus apparent that roots infected by the fungus under three N forms conditions exhibited different cellular responses. In the presence of NH_4^+, the fungus causes more severe oxidative damage to the root tissues and the ingress was accompanied by a marked burst of H_2O_2 production. In contrast, a sudden increase of H_2O_2 production was detected at the second time point in the presence of NO_3^-. This pattern probably reflected a delayed onset of the pathogenic interaction. It appears that the fungus, grown on organic N, induced a similar defense process but with a milder oxidative burst. Altogether, H_2O_2 changes seen during the early infection stage suggested a dynamic symbiosis ranging from parasitic to mutualistic.

Under organic N condition, root fresh weight, total root number, total root length, and fresh shoot weight all increased after inoculation with *C. hobsonii* (Student's two-sample t test, $p = 0.015$, $p < 0.001$, $p = 0.017$, and $p = 0.074$, respectively) (Figures 1E–1H). Notably, N concentrations in the shoots and roots of inoculated plants were higher compared with mock-inoculated plants (Student's two-sample t test, $p < 0.001$ and $p = 0.021$, respectively) (Figure 1I). In comparison, p concentration only increased slightly in roots (Student's two-sample t test, $p = 0.079$), whereas p concentration in shoots and potassium concentration in whole plants were not affected by the fungus (Figure 1I).

In the microcosm system used to track the transfer of ^{15}N between partners, the compartments allowed mycelia growth over the barrier, but roots could not penetrate ^{15}N containing compartment (Figure 1J). Therefore, the uptake of ^{15}N in the root of the plant was entirely dependent on transport via the fungal mycelium. *C. hobsonii*-inoculated plants were cultivated in the presence of ^{15}N-labeled glycine for 4 weeks. Evidence for the incorporation of ^{15}N in both stems and leaves indicated ^{15}N translocation from the fungus to the aboveground parts of the host plant (Figure 1K). As similar isotope signatures were not detected in control plants, leakage of ^{15}N from the small Petri dish containing the isotope could be excluded. Additionally, API-ZYM assays revealed a strong trypsin reaction in mycelia grown in the presence of organic N, whereas the same assay was negative when the fungus was grown on mineral N (Figure S4; STAR Methods). These data implied a trypsin-like proteolytic activity that degrades organic N before it is being provided to the plants. This was consistent with the notion of a mineralization process taking place in *C. hobsonii* before the N was transferred to the plants.

Mycelia fed on organic N trigger adventitious rooting on detached leaves

Fungal development and plant responses were also examined using detached leaves. The leaves showed no necrotic symptoms, and adventitious rooting was initiated at the cut end of the petioles in the presence of *C. hobsonii* grown on organic N. In these cultures, after 1 week, hyphae were already approaching the leaf margin and petioles (Figure 2A). After 4 weeks of inoculation, sometimes, even ECM-like structures were observed on newly emerging roots (Figure 2B). In contrast, when leaf tissues were incubated in media supplemented with mineral N, the pre-grown *C. hobsonii* damaged the detached leaves (Figure 2A). The latter were completely bleached when the fungus was cultured in the presence of NH_4^+, whereas *C. hobsonii* caused some decay of the detached leaves when grown under NO_3^- condition. Leaves from the three control groups remained almost completely green and healthy but failed to develop adventitious roots.

We decided to investigate further how detached leaves respond to exposure to soluble fungal metabolites released into the media. The fungal colonies were pre-grown on a cellophane membrane covering the medium. The membranes containing the attached mycelia were removed with forceps after 2 weeks. This way water-soluble metabolites that diffused through the cellophane membrane were retained in the agar medium. Detached leaves showed a substantial increase of rooting efficiency when plated on the agar medium that previously supported the fungus in the presence of organic N (Figure S5). In contrast, leaves placed on agar media that previously had *C. hobsonii* growing under mineral N conditions were susceptible to the deleterious effects described above (Figure S5). These observations suggested that *C. hobsonii*, when grown under either NH_4^+ or NO_3^- conditions, produce diffusible compound(s) inhibiting plant development (Figure S5).

The crude extracts of *C. hobsonii* grown on organic N promote poplar cell growth

The aim of this series of experiments was to ascertain whether crude extracts of the fungus grown utilizing the three distinct N forms had any effect on poplar cell growth. Such analysis may provide clues regarding how various N forms regulate fungal primary or secondary metabolism. Crude extracts were derived from both lyophilized mycelia and filtered culture media. When these crude extracts were derived from mycelia grown on organic N medium, a significant increase in the size of the cultured cells was seen after 10 days (ANOVA, $F = 207.331$, $df = 277$, $p < 0.001$). A significant increase in cell density was also observed at this time point (ANOVA, $F = 14.818$, $df = 10$, $p = 0.002$). A similar trend was seen when using extracts of the filtered culture media. Both cell size (ANOVA, $F = 8.977$, $df = 293$, $p < 0.001$) and cell density (ANOVA, $F = 13.381$, $df = 11$, $p = 0.017$) showed significant increases after 10 days. In contrast, both poplar cell density and size were severely reduced when the cells were exposed to extracts from mycelial or filtrates of NO_3^--grown *C. hobsonii*, suggesting the release of toxic or inhibitory compound(s) (Figures 2C–2G). The growth of suspension cells was not significantly affected by crude extracts derived from NH_4^+-grown mycelia when compared with the control group.

(D–G) Comparison of the effect of crude fungal extracts on the proliferation and size of suspension cells (six time points). Statistical significance is calculated using an ANOVA. Different lowercase letters are indicating significance levels. Cell suspensions are grown at 26°C in darkness with shaking at 110 rpm/min.
(H) Phytohormone concentrations in extracts from mycelia and filtered culture medium. Error bars represent SD of the mean values from three biological replicates. IAA, indole-3-acetic acid; IBA, indole-3-butyric acid; ABA, abscisic acid; TZR, *trans*-zeatin-riboside; SA, salicylic acid; MeSA, methyl salicylic acid; JA, jasmonic acid; MeJA, methyl jasmonic acid; GA3, gibberellin A3.
See also Figure S5.

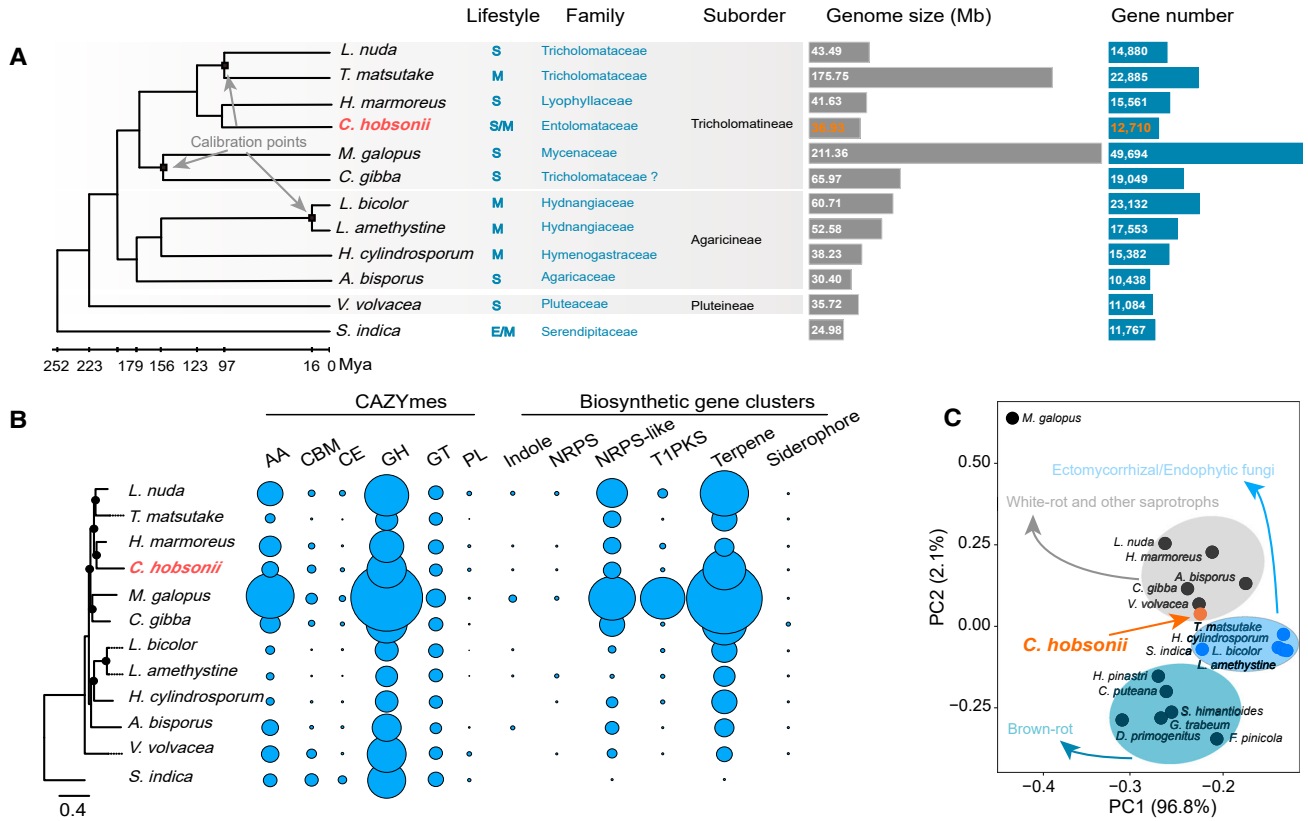

Figure 3. Genome overview of *C. hobsonii* and related species and comparative phylogenomics

(A) Phylogenomic species tree constructed with 1,654 core orthologous single-copy genes using MrBayes v3.1.2 using the GTR model of substitution, with gamma-distributed rate variation. Three calibration points are used to generate a time-calibrated phylogeny. Members within Agaricales across eight families, possessing lifestyle of saprotrophic (S) and mycorrhizal fungi (M), are indicated. *S. indica*, either endophytic (E) or mycorrhizal, is selected as an outgroup. Calibration points are indicated by gray arrows. Gene numbers and genome size for all species are shown on the right panel.

(B) The number of genes (secreted and non-secreted) annotated as CAZymes, as well as the number of BGCs involved in secondary metabolite biosynthesis are indicated as bubbles. The bubble size is proportional to the number of genes from each functional family. The left panel shows the maximum likelihood phylogeny. Branches with 100% bootstrap support are indicated by filled in black circles.

(C) Principal component analysis (PCA) inferred from the secreted CAZymes of 18 fungal species. Saprotrophic fungi (gray and dark blue), with an exception of *M. galopus*, are well separated from mutualistic fungi (blue). Within the white-rot and other saprotrophic group, *C. hobsonii* is the only species nearest to the mutualistic group. *L. nuda*, *Lepista nuda*; *T. matsutake*, *Tricholoma matsutake*; *H. marmoreus*, *Hypsizygus marmoreus*; *M. galopus*, *Mycena galopus*; *C. gibba*, *Clitocybe gibba*; *L. bicolor*, *Laccaria bicolor*; *L. amethystina*, *Laccaria amethystina*; *H. cylindrosporum*, *Hebeloma cylindrosporum*; *A. bisporus*, *Agaricus bisporus*; *V. volvacea*, *Volvariella volvacea*; *S. indica*, *Serendipita indica*; *S. himantioides*, *Serpula himantioides*; *C. puteana*, *Coniophora puteana*; *D. primogenitus*, *Dacryopinax primogenitus*; *F. pinicola*, *Fomitopsis pinicola*; *G. trabeum*, *Gloeophyllum trabeum*; *H. pinastri*, *Hydnomerulius pinastri*.

By using HPLC-MS profiling, a total of ten common phytohormones were detected in mycelial extracts. Indole-3-acetic acid (IAA) and salicylic acid (SA) were the most abundant metabolites (Figure 2H). In addition, other phytohormones were detected at a much lower concentration in the culture filtrates. Unfortunately, unambiguous identification of the toxic compound(s) produced by NO_3^--grown *C. hobsonii* was not possible due to the lack of available reference libraries.

Features of saprotrophic and mutualistic lifestyles are imprinted in *C. hobsonii* genome

We next sought to determine if the gene repertoire of *C. hobsonii* displayed any footprint of the ECM mutualism, i.e., a restricted set of genes coding for PCWDEs and toxin biosynthesis enzymes. To our knowledge, this was the first phylogenomic analysis of a member of the Entolomataceae family. *C. hobsonii* was placed as a sister clade to *Hypsizygus marmoreus*, a typical saprotrophic species (Figure 3A). Of note, we found that the Lyophyllaceae and Tricholomataceae could not be distinguished clearly due to the polyphyletic nature of the *Clitocybe* genus. This observation was consistent with previous studies.[37–39] Despite this discrepancy, all members from Lyophyllaceae, Tricholomataceae, Entolomataceae, and Mycenaceae fell within the suborder Tricholomatineae,[40] encompassing both mycorrhizal and saprotrophic taxa. The most recent common ancestor of *C. hobsonii* and *H. marmoreus* was estimated to have existed *ca.* 101 Ma (95% CI, 97.7–123.0) (Figure 3A).

We then characterized the repertoire of genes coding for PCWDEs and biosynthetic gene clusters (BGCs), which play an important role in interactions between plants and fungi. Compared with ECM fungi, *C. hobsonii* genome encoded a larger set of carbohydrate-active enzyme (CAZyme) genes

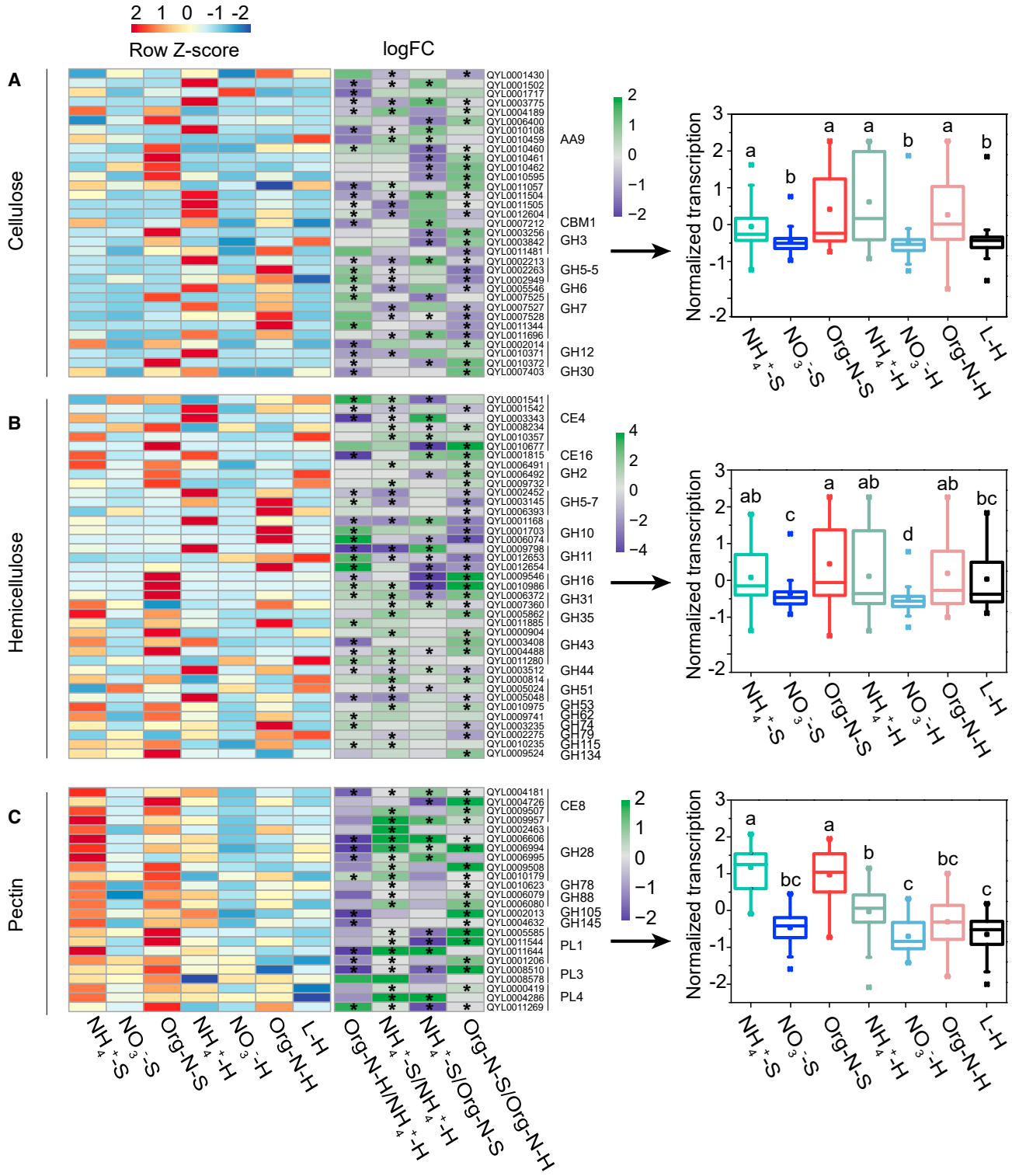

Figure 4. Transcriptional signature of fungal genes related to plant cell-wall degradation

(A) Expressed genes involved in the deconstruction of cellulose.

(B) Expressed genes involved in the deconstruction of hemicellulose.

(C) Expressed genes involved in the deconstruction of pectin. *Z* score-transformed expression data are visualized by heatmaps in each cluster (left panel). The color key from blue to red indicates low to high gene expression. Gene expression fold changes (green, upregulated; violet, downregulated) are calculated for each pairwise comparison (middle panel). Genes are considered to be significantly differentially expressed at a false discovery rate (FDR) < 0.05, |logFC| ≥ 1 (indicated by an asterisk). Bar plots of the averaged normalized expression values for each cluster of CAZymes genes (right panel) are generated. Statistical

(legend continued on next page)

(348 genes), similar to, or slightly lower than, those of saprotrophic and endophytic fungi, such as *H. marmoreus*, *Lepista nuda*, *Clitocybe gibba*, *Volvariella volvacea*, and *S. indica* (Figure 3B). A total of 36 BGCs were identified. This number was higher than that reported in ECM and endophytic fungi but less than would be expected in saprotrophic fungi. We applied principal component analysis (PCA) to the set of CAZyme repertoires. To this end, we additionally included six brown-rot taxa for comparison. The first two PCs together explained 98.9% of the total variance. Clear separation of saprotrophic and ECM/endophytic groups was seen along PC2, and it also appeared that ECM/endophytic groups were intermediate between white-rot and soil decomposer saprotrophs and brown-rot fungi (Figure 3C). In this analysis, within the white-rot and other saprotrophic group, *C. hobsonii* was the species nearest to the ECM/endophytic group, pointing to its dual saprotrophic/mutualistic lifestyle.

Transcriptomic evidence for maintenance and breakdown of mutualism

The mycelial transcriptional profiles of the fungus grown on the three N sources, litters, and *in planta* were analyzed using RNA sequencing. Overall the expression of 6,834 genes was significantly altered (moderated t test, $|\log FC| \geq 1$, false discovery rate [FDR] < 0.05), accounting for 53.77% of all predicted genes. This represents the total number of different expression genes (DEGs) found for each pairwise comparison between cultured mycelia across all six conditions and those cultured on litters (Table S1). To narrow down our analysis, we focused on the differential expression of transcripts coding for secreted CAZymes, core BGC genes, and genes involved in N metabolism, including N uptake, transport, and amino acid hydrolysis.

A closer look at the expressions of PCWDEs revealed that a vast array of genes encoding cellulolytic, hemicellulolytic, and pectin degradation enzymes showed an altered expression when RNA was derived from mycelia grown *in vitro* and *in planta* on organic N (Figures 4A–4C). For instance, several transcripts of *GH5-7* (QYL0002452, QYL0003145, and QYL0006393) and *GH7* (QYL0007527, QYL0007528, QYL0011344, and QYL0011696) were downregulated *in planta*. Conversely, the abundance of transcripts of genes including *AA9* (QYL0004189, QYL0006400, QYL0010460, QYL0010461, QYL0010462, QYL0010595, and QYL0011057), *GH3* (QYL0003256 and QYL0003842), *GH12* (QYL0002014 and QYL0010372), *GH16* (QYL0009546 and QYL0010986), and *GH31* (QYL0006372) was preferentially expressed in the symbiotic stage (Figures 4A and 4B). Similarly, genes related to pectin degradation including *CE8* (QYL0004181, QYL0009507, and QYL0009957), *GH28* (QYL0006994, QYL0009508, and QYL0010179), and several members in the PL family (QYL0005585, QYL0011544, QYL0001206, and QYL0008510) were selectively expressed *in planta*, whereas they were barely detected in the absence of the host (Figure 4C). Some of these PCWDEs were likely to be required for plant cell-wall loosening. Among these, the roles of AA9, GH28, and GH12 in modification of cell wall have been functionally verified.[41–44] Interestingly, the expression of these pectin-digesting genes, e.g., *GH28* (QYL0006606, QYL0006994, and QYL0006995), *CE8* (QYL0009507 and QYL0009957), and *PL1* (QYL0011644), was also highly induced *in planta* under NH_4^+ condition (Figure 4C). The reciprocal association between logFC and FDR of these genes across four pairwise groups was shown. Furthermore, by plotting the average normalized expression values of each dataset, we observed that genes involved in the degradation of plant cell wall were expressed at much higher abundance under NH_4^+ and organic N conditions, both *in vitro* and *in planta* (Figures 4A–4C). In conclusion, the secreted PCWDE genes of *C. hobsonii* showed contrasting expression profiles in free-living mycelia and *in planta*, when grown on organic N or NH_4^+.

Looking at the distribution of 39 core BGC genes across different scaffolds (Figure 5A), we observed that their expression patterns were distinct, with almost no overlap between gene expression seen *in planta* and *in vitro* stages under organic N condition (Figure 5B). It is worth noting that a suite of core BGC genes showed much higher expression in NO_3^--fed mycelia. For example, transcripts encoding terpene synthase and non-ribosomal peptide synthetase (NRPS) located on the scaffold 4 (QYL0008032 and QYL0008086), scaffold 8 (QYL0001787), and scaffold 12 (QYL0000065) were significantly more abundant *in vitro*, indicating an improved capability to synthesize secondary metabolites. However, most core BGC genes were either moderately expressed or expressed at low levels when the fungus was grown utilizing NH_4^+, both *in vitro* and *in planta*.

Next, the transcriptional profile of N assimilation pathways was analyzed (Figure 6A). As expected, genes coding for nitrate reductase (NR) (QYL0010885) and nitrite reductase (Nir) (QYL0011931) were upregulated by NO_3^- depletion (Figure 6B). The pathway-specific transcription factor, *nit-4* (QYL0010058), involved in N utilization was also significantly upregulated both *in planta* and *in vitro* under NO_3^- conditions (Figure 6B). Genes encoding for NO_3^- transporters (NRTs) were not found in the *C. hobsonii* genome.[45] It is unlikely that these genes were missed because of incomplete genome coverage, as the *C. hobsonii* genome assembly encompasses 98.4% of the conserved Basidiomycota single-copy gene set.[45] Thus, the absence of NRTs provided a likely explanation for the very poor growth of the fungus on NO_3^- as the sole N source. Three NH_4^+ transporter (AMT) transcripts (QYL0003392, QYL0000700, and QYL0000737) showed similar expression patterns (Figure 6B). Regarding amino acid uptake, a greater proportion of amino acid transporter genes (AAT) (QYL0004305, QYL0005669, QYL0008241,

significance is calculated using the Mann-Whitney U test. Different lowercase letters indicate significance level ($p < 0.05$). Genes with maximum FPKM values less than 5 across all samples are excluded for analysis. NH_4^+-S, *in planta* gene expression under NH_4^+ condition; NO_3^--S, *in planta* gene expression under NO_3^- condition; Org-N-S, *in planta* gene expression under organic N condition; NH_4^+-H, *in vitro* (free-living mycelia) gene expression under NH_4^+ condition; NO_3^--H, *in vitro* gene expression under NO_3^- condition; Org-N-H, *in vitro* gene expression under organic N condition; L-H, *in vitro* gene expression cultured on litters. The same abbreviations are shown below. GHs, glycosyl hydrolases; GTs, glycosyl transferases; CBMs, chitin-binding motifs; CEs, carbohydrate esterases; AAs, auxiliary activities; PLs, polysaccharide lyases. In total, 21 RNA samples are prepared.
See also Table S3.

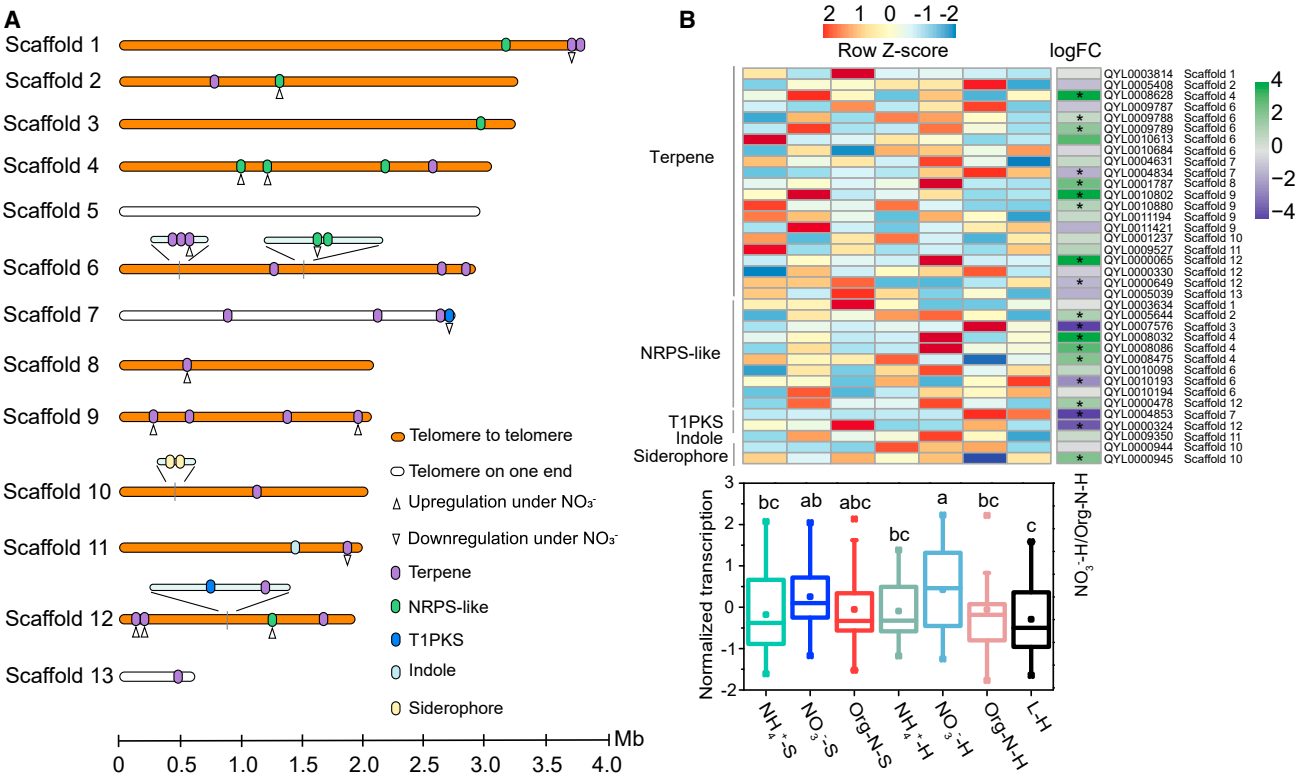

Figure 5. Transcriptional signature of secondary metabolite biosynthetic genes

(A) Diagram illustrating the location of 39 core BGC genes on scaffolds.

(B) *Z* score-transformed expression data, visualized by heatmaps. The color key from blue to red indicates low to high gene expression. Gene expression fold changes (green, upregulated; violet, downregulated) are calculated for each pairwise comparison (middle panel). Genes are considered to be significantly differentially expressed at a false discovery rate (FDR) < 0.05, |logFC| ≥ 1 (indicated by an asterisk). For simplicity, only one pairwise comparison of NO_3^--H versus Org-N-H is shown. Bar plots of averaged normalized expression values are generated. Statistical significance is calculated using the Mann-Whitney U test. Different lowercase letters indicate the level of significance ($p < 0.05$). Genes with maximum FPKM values less than 5 across all samples are excluded for analysis. See also Table S3.

and QYL0008968) was upregulated in the presence of NO_3^-. In contrast, under organic N, their expressions were slightly or even strongly downregulated in symbiotic roots (Figure 6B). Sub-clustering analysis was conducted to determine whether there were transcriptionally distinct states for organic N-fed mycelia (Figure S6). This analysis identified ten distinct sub-clusters. Of these, sub-cluster 9 was particularly characteristic, where the expression levels of 536 genes were much higher in organic N-fed mycelia than in those fed on mineral N (Figure 6C). According to the results of Kyoto encyclopedia of genes and genomes (KEGG) pathway enrichment analysis, the upregulated DEGs were significantly enriched in the pathway associated with valine, leucine, and isoleucine degradation (Figure 6D). These findings imply that an organic N mineralization process is already active before the mutualistic interaction occurs.

Finally, to identify more additionally important DEGs linked to lifestyle-related traits, we narrowed down the comparison to genes exhibiting the highest fold changes, some showing >100-fold change in expression. For example, the striking overexpression of two genes coding for cerato-platanin (QYL0008591 and QYL0006142) and M35 deuterolysin metalloproteases (QYL0010117) was seen in the presence of NH_4^+ or NO_3^-, respectively. These drastic changes in expression levels were seen both *in vitro* and *in planta*. These two genes are highly induced during pathogenic interactions.[46,47] Additionally, we found that transcripts coding for clitocypin cysteine proteinase inhibitor (QYL0006421) were overrepresented during the mutualistic interaction when compared with the levels seen during mineral N feeding. This pattern was also recorded in poplar ECM symbioses[15,48] (Figure S7). These results provide the evidence of a striking metabolic reprogramming during the parasitism-mutualism shift.

DISCUSSION

The work presented here provides several lines of evidence supporting the existence of a novel, unexpected mechanism, driven by available N forms, for the maintenance and breakdown of a plant-fungus mutualism. Here, we show that organic N facilitates the accommodation of *C. hobsonii* in roots, where the fungus behaves as a facultative ECM fungus, whereas both NO_3^- and NH_4^+ may easily render this association parasitic. This supports previous reports that N forms govern the development of host-microbe relationships. Thus, such conditional mutualism is likely more widespread than previously thought.

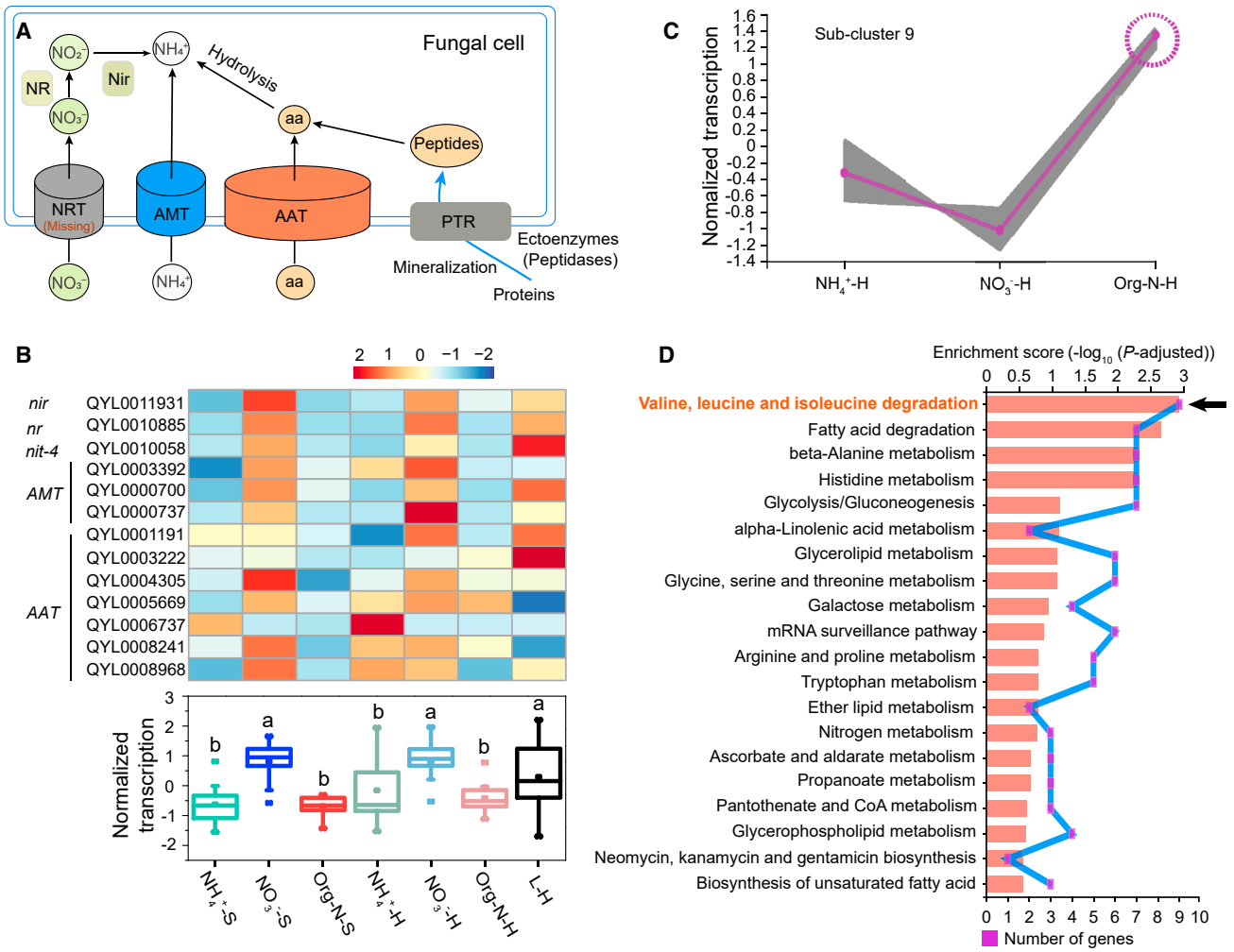

Figure 6. Transcriptional signature of fungal N transporters and metabolism

(A) The diagram illustrates N transportation, mineralization, and metabolism in fungi.

(B) Heatmap showing the expression profile of genes coding for NO_3^- reductases (Nr), nitrite reductases (Nir), NIT-4, ammonia transporter (AMT), and amino acid transporter (AAT). The color key from blue to red indicates low to high gene expression. Bar plots of the averaged normalized expression values are generated. Statistical significance is calculated using the Mann-Whitney U test. Different lowercase letters indicate the level of significance ($p < 0.05$). Genes with maximum FPKM values less than 5 across all samples are excluded for analysis. PTR, peptide transporter.

(C) Gene expression model of sub-cluster 9, showing the highest average normalized expression level under organic N condition indicated by a violet dotted circle. All genes with similar expression patterns are clustered by complete linkage clustering based on the average Euclidean distance (see Figure S6).

(D) KEGG pathway enrichment analysis of expressed genes from the sub-cluster 9. Bars show the enrichment score ($-\log_{10}$ (p-adjusted)) of the pathways in the dataset. In all cases, the valine, leucine, and isoleucine degradation pathway with the highest enrichment score is indicated by a black arrow.

See also Figure S6 and Table S3.

Our work extends previous ecological observations pointing out the negative impact of mineral N on plant-fungus symbioses. By building a novel experimental model system, we are able to infer causal mechanisms underlying such scenario. A key point is that N form-mediated maintenance and/or breakdown of mutualism is tightly regulated by multi-faceted mechanisms. One of the main causes of the mutualism-parasitism shift could be an extensive reprogramming of fungal metabolism in response to exogenous organic or mineral N supply. *C. hobsonii* growth well on organic N, utilizing either protein or amino acids, suggesting its pre-adaptation to substrates enriched in organic N sources. This mechanism is known to facilitate ECM establishment.[49] Intriguingly, mycelial and culture filtrate extracts under organic N growth condition are beneficial to poplar cell growth. This may be related to the ability of *C. hobsonii* to synthesize IAA. It should be noted that although the fungus also produces high level of SA, its role in promoting mutualism remains unknown. More surprisingly, NO_3^- uptake by *C. hobsonii* appears rather limited due to the lack of NRT genes. A similar phenomenon is described in several ECM fungi and in the endophyte *S. indica*.[13,46,50] N limitation is recognized as a key signal for activating the virulence of plant pathogens.[51] Although we are not able to identify the toxic metabolites released by *C. hobsonii* into its growth medium, it appears that NO_3^- induces the production of compounds highly toxic to poplar cells. This mechanism may have far reaching implications in

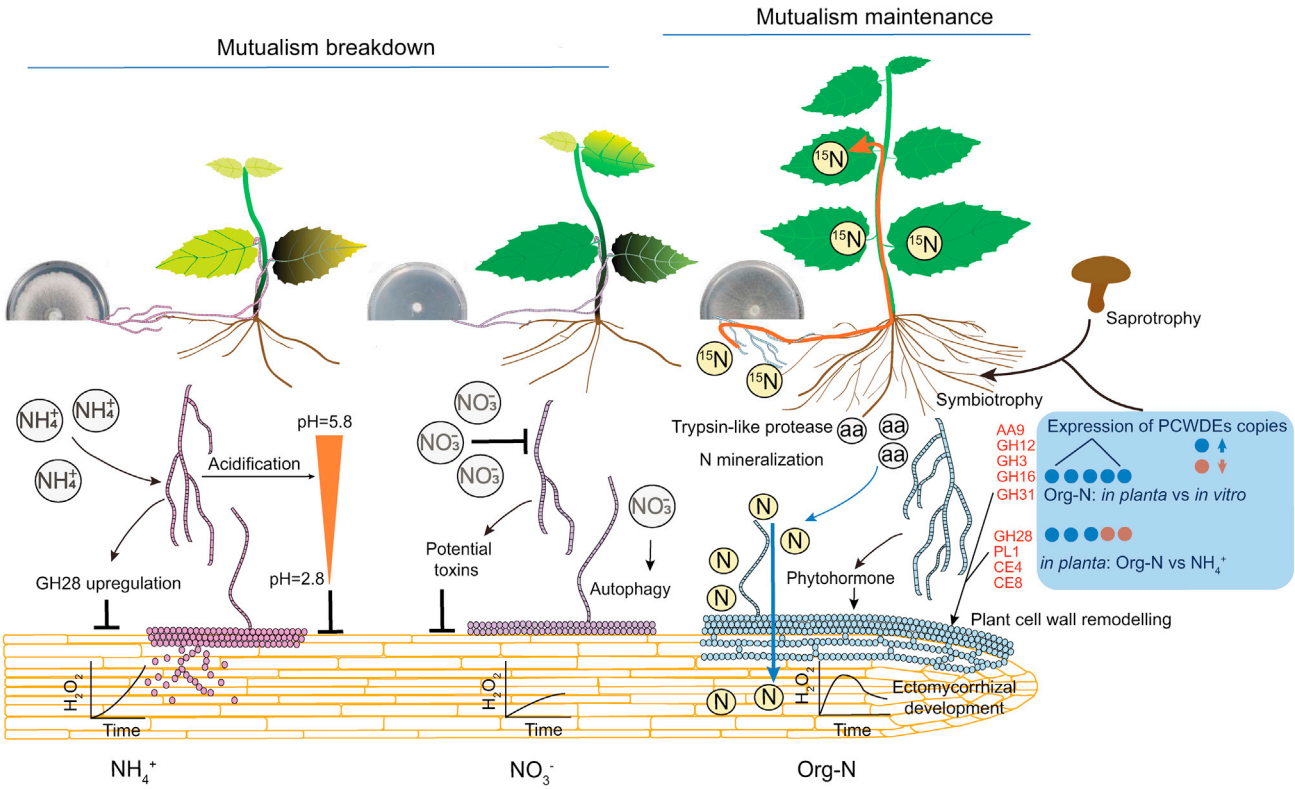

Figure 7. A schematic illustration of N form-mediated mutualism-parasitism transition in the poplar-*C. hobsonii* association

It is proposed that fungal physiological behavior and gene expression are remodeled when sensing different N forms, ultimately governing the outcome of interaction. Under NH_4^+ condition, acidification of the growth substrate and upregulation of genes coding for pectin-degrading enzymes (such as GH28 and PL1) are recorded, potentially accounting for the breakdown of mutualism. In this scenario continuous high H_2O_2 production suggests that the root cells are destroyed. Under NO_3^- condition, the fungus lacks NO_3^- transporter genes and could not assimilate NO_3^-. Such N starvation leads to the overexpression of genes related to N uptake, metabolism, transportation, and autophagy. Genes involved in secondary metabolite biosynthesis (such as terpene synthase and NRPS) are highly induced, leading to potential toxin production, as evidenced by strong inhibition of poplar cell growth exposed to crude extracts. On organic N, the fungus mineralizes the amino acids to allow plants to have sufficient access to available N. In addition, phytohormones, mainly IAA, produced by the fungus, could improve root development. Genes encoding AA9, GH3, GH12, GH16, GH31, GH43, PL1, CE4, and GH28 are clearly upregulated during symbiotic interaction. This transcriptional pattern contributes to the plant cell-wall remodeling and development of ectomycorrhizal structures, indicating that *C. hobsonii* is experiencing an intermediate status between obligate saprotrophy and symbiotrophy. Such facultative symbiosis is consistent with a tight control of H_2O_2 production in roots. Among these, the abundance of pectin-degrading enzymes (GH28, PL1, and CE8) with distinct expression patterns during functional divergence after exposure to NH_4^+ or organic N is likely to be central to the transition from parasitism to mutualism.

the pathogenic behavior of *C. hobsonii*. The upregulation of numerous transcripts coding for terpene synthase and NRPS-like genes may be a mechanism leading to mycotoxin biosynthesis.[52,53] Another intriguing, albeit little studied aspect of fungal physiology is the abundant expression of genes related to N uptake, metabolism, and transportation *in vitro* and *in planta* in the presence of NO_3^-. N starvation while growing on NO_3^- may trigger autophagy in *C. hobsonii*, leading to an increased expression of N transporters, with the aim to reallocate nutrients within the mycelium.[54,55] Another plausible explanation is that translocation of N from plant to fungus could also happen when N is supplied in the form of NO_3^-.[56]

The overall similarity of the repertoire of PCWDE genes between *C. hobsonii* and typical ECM fungi supports a convergent evolution.[57,58] This study, as well as our previous work,[35] provides experimental evidence of the endophytic and mycorrhizal potential of *C. hobsonii*. These observations may fit well the "waiting room" hypothesis that the fungus has a dual trophic status (saprotrophy and endophytism). *C. hobsonii* has the potential to behave like an ECM associate when facing suitable hosts and growth conditions.[59] Thus, both genomic features and experimental data likely support the contention that an incomplete switch from saprotrophy to symbiotrophy is taking place in *C. hobsonii*. A set of PCWDE genes acting on cellulose and hemicellulose are strikingly upregulated in the presence of organic N, indicating the induction of activities for plant cell-wall degradation. Cellophane membrane decay further supports the penetrative capacity of organic N-fed mycelia, thereby promoting root colonization by *C. hobsonii*. Not surprisingly, the expression of these genes is drastically downregulated in the presence of plant roots, with a concomitant upregulation of another subset of genes. Among these, 6 copies of copper-dependent lytic polysaccharide monooxygenase (LPMO-AA9 family) genes are abundantly expressed during beneficial interactions. Genomic and transcriptomic analyses support the notion that the AA9 family might be acting as a genetic determinant of fungal mutualism[60] and is induced during ECM development.[42] Unexpectedly, most genes involved in pectin hydrolysis are highly expressed

in planta. This pattern seems to fine-tune the attenuation of plant immune responses, helping to establish and develop successful ECM symbioses.[61] However, at this stage, we are not able to identify specific genes involved in this process. The role of plant immune responses is further supported by 3,3′-diaminobenzidine (DAB) staining, demonstrating that H_2O_2 production significantly decreases in the roots by a later time point. This raises the possibility that the tight control of H_2O_2 production could be crucial for establishing beneficial interactions.[62] The presence of fairly aggressive enzymes affecting the host plant is comparable with that found in ericoid and orchid mycorrhizal fungi and the ECM fungus *Tuber melanosporum*.[57,58,63,64] Taken together, the differential PCWDE profiles of *C. hobsonii* observed during the mutualistic interaction suggest a "gentle" remodeling of the plant cell wall. However, we cannot rule out possible further changes beyond the time points used in our work.

Mechanisms leading to the breakdown of mutualistic interaction under NH_4^+ condition are distinct. In accordance with previous reports, in the presence of NH_4^+, a rapid decrease of the pH of the medium is recorded.[65,66] This low pH environment could favor optimal fungal growth,[66] whereas upregulating the expression of certain PCWDEs ultimately contributes to pathogenicity.[67,68] Genes encoding enzymes acting on pectin (CE8, GH28, and PL1) are expressed at higher levels *in planta*. The ongoing H_2O_2 bursts seen in the roots probably result from pectin breakdown caused by these polygalacturonases. An intriguing point is that other transcripts from each of the above three gene families are also significantly upregulated during the mutualistic interaction, suggesting a functional divergence of multiple duplicated genes, as shown in pine and poplar ECMs.[44,69] This could be due to diversifying selection or horizontal gene transfer.[70,71] Presumably, gene expression changes due to copy-number variations within several CAZyme families may correlate with their dual nature, exhibiting either mutualistic or pathological traits.[69]

In sum, the increasing anthropogenic N deposition may thus possibly alter the balance between saprotrophism, parasitism, and mutualism in many plant-microbe interactions. Our work further highlights the serious concern that if these root-inhabiting fungi are suppressed by NO_3^- leaching into forest ecosystems, there will be a particular risk of increasing disruption of belowground mutualism, and a dangerous negative feedback can develop over time (Figure 7). The biological and practical implications of these findings are 3-fold: (1) N forms should be recognized as important trophic factors regulating mutualism. (2) The preference for organic N among ECM fungi, DSE, and Sebacinales endophytes supports the concept that N forms in forest soils play a key role in shaping the contributions of root-associated fungal guilds. (3) The potential utilization of fungi favoring organic N sources may be capitalized upon in sustainable forest management relying on organic rather than mineral fertilizers.

STAR★METHODS

Detailed methods are provided in the online version of this paper and include the following:

SUPPLEMENTAL INFORMATION

Supplemental information can be found online at https://doi.org/10.1016/j.cub.2022.10.054.

ACKNOWLEDGMENTS

This work was funded by Fundamental Research Funds for the Central Nonprofit Research of Chinese Academy of Forestry (CAFYBB2020QB002), National Key Research and Development Program of China (2022YFD2201900), and National Natural Science Foundation of China (no. 31901290 and 31722014). Research in FMM laboratory is funded by the Laboratory of Excellence Advanced Research on the Biology of Tree and Forest Ecosystems (ARBRE; grant ANR-11-LABX-0002-01). We are grateful to Prof. Guanzheng Qu (Northeast Forestry University, China) for providing the poplar cells.

AUTHOR CONTRIBUTIONS

Z.Y., L.P., and F.M. conceived the experiments. L.P., Yan Zhang, X.Z., Yuwei Zhang, and Z.L. performed the experiments and analyzed the data. Z.Z., K.W., and Yuwei Zhang assisted with WGA staining and fungal extract preparation. I.S.D., C.P.K., and Y.W. assisted with data interpretation. Z.Y., F.M., and L.P. wrote the article; all authors contributed to the final draft.

DECLARATION OF INTERESTS

The authors declare no competing interests.

Received: May 20, 2022
Revised: September 19, 2022
Accepted: October 25, 2022
Published: November 18, 2022

REFERENCES

1. Brader, G., Compant, S., Vescio, K., Mitter, B., Trognitz, F., Ma, L.J., and Sessitsch, A. (2017). Ecology and genomic insights into plant-pathogenic and plant-nonpathogenic endophytes. Annu. Rev. Phytopathol. *55*, 61–83.

2. Cheng, Y.T., Zhang, L., and He, S.Y. (2019). Plant–microbe interactions facing environmental challenge. Cell Host Microbe *26*, 183–192.
3. Álvarez-Loayza, P., White, J.F., Jr., Torres, M.S., Balslev, H., Kristiansen, T., Svenning, J.C., and Gil, N. (2011). Light converts endosymbiotic fungus to pathogen, influencing seedling survival and niche-space filling of a common tropical tree, *Iriartea deltoidea*. PLoS One *6*, e16386.
4. Newland, J.A., and DeLuca, T.H. (2000). Influence of fire on native nitrogen-fixing plants and soil nitrogen status in ponderosa pine-Douglas fir forests in western Montana. Can. J. For. Res. *30*, 274–282.
5. Sachs, J.L., and Simms, E.L. (2006). Pathways to mutualism breakdown. Trends Ecol. Evol. *21*, 585–592.
6. Hiruma, K., Gerlach, N., Sacristán, S., Nakano, R.T., Hacquard, S., Kracher, B., Neumann, U., Ramírez, D., Bucher, M., O'Connell, R.J., et al. (2016). Root endophyte *Colletotrichum tofieldiae* confers plant fitness benefits that are phosphate status dependent. Cell *165*, 464–474.
7. Sun, K., Zhang, W., Yuan, J., Song, S.L., Wu, H., Tang, M.J., Xu, F.J., Xie, X.G., and Dai, C.C. (2020). Nitrogen fertilizer-regulated plant–fungi interaction is related to root invertase-induced hexose generation. FEMS Microbiol. Ecol. *96*, fiaa139.
8. Imin, N., Mohd-Radzman, N.A., Ogilvie, H.A., and Djordjevic, M.A. (2013). The peptide-encoding CEP1 gene modulates lateral root and nodule numbers in *Medicago truncatula*. J. Exp. Bot. *64*, 5395–5409.
9. Bisseling, T., and Scheres, B. (2014). Plant Science. Nutrient computation for root architecture. Science *346*, 300–301.
10. Laffont, C., Ivanovici, A., Gautrat, P., Brault, M., Djordjevic, M.A., and Frugier, F. (2020). The NIN transcription factor coordinates CEP and CLE signaling peptides that regulate nodulation antagonistically. Nat. Commun. *11*, 3167.
11. Shi, J., Zhao, B., Zheng, S., Zhang, X., Wang, X., Dong, W., Xie, Q., Wang, G., Xiao, Y., Chen, F., et al. (2021). A phosphate starvation response-centered network regulates mycorrhizal symbiosis. Cell *184*, 5527–5540.e18.
12. Müller, L.M., and Harrison, M.J. (2019). Phytohormones, miRNAs, and peptide signals integrate plant phosphorus status with arbuscular mycorrhizal symbiosis. Curr. Opin. Plant Biol. *50*, 132–139.
13. Nygren, C.M., Eberhardt, U., Karlsson, M., Parrent, J.L., Lindahl, B.D., and Taylor, A.F. (2008). Growth on nitrate and occurrence of nitrate reductase-encoding genes in a phylogenetically diverse range of ectomycorrhizal fungi. New Phytol. *180*, 875–889.
14. Plett, K.L., Singan, V.R., Wang, M., Ng, V., Grigoriev, I.V., Martin, F., Plett, J.M., and Anderson, I.C. (2020). Inorganic nitrogen availability alters *Eucalyptus grandis* receptivity to the ectomycorrhizal fungus *Pisolithus albus* but not symbiotic nitrogen transfer. New Phytol. *226*, 221–231.
15. Plett, K.L., Snijders, F., Castañeda-Gómez, L., Wong-Bajracharya, J.W., Anderson, I.C., Carrillo, Y., and Plett, J.M. (2022). Nitrogen fertilization differentially affects the symbiotic capacity of two co-occurring ectomycorrhizal species. Environ. Microbiol. *24*, 309–323.
16. Lekberg, Y., Arnillas, C.A., Borer, E.T., Bullington, L.S., Fierer, N., Kennedy, P.G., Leff, J.W., Luis, A.D., Seabloom, E.W., and Henning, J.A. (2021). Nitrogen and phosphorus fertilization consistently favor pathogenic over mutualistic fungi in grassland soils. Nat. Commun. *12*, 3484.
17. Reuter, R., Ferlian, O., Tarkka, M., Eisenhauer, N., Pritsch, K., and Simon, J. (2021). Tree species rather than type of mycorrhizal association drive mineral and organic nitrogen acquisition in tree-tree interactions. Tree Physiol. *41*, 2096–2108.
18. Wu, Y., Kwak, J.H., Karst, J., Ni, M., Yan, Y., Lv, X., Xu, J., and Chang, S.X. (2021). Long-term nitrogen and sulfur deposition increased root-associated pathogen diversity and changed mutualistic fungal diversity in a boreal forest. Soil Biol. Biochem. *155*, 108163.
19. Finlay, R.D., Frostegård, A., and Sonnerfeldt, A.-M. (1992). Utilization of organic and mineral nitrogen sources by ectomycorrhizal fungi in pure culture and in symbiosis with *Pinus contorta* Dougl. ex Loud. New Phytol. *120*, 105–115.
20. Vaario, L.M., Sah, S.P., Norisada, M., Narimatsu, M., and Matsushita, N. (2019). *Tricholoma matsutake* may take more nitrogen in the organic form than other ectomycorrhizal fungi for its sporocarp development: the isotopic evidence. Mycorrhiza *29*, 51–59.
21. Huberman, L.B., Wu, V.W., Kowbel, D.J., Lee, J., Daum, C., Grigoriev, I.V., O'Malley, R.C., and Glass, N.L. (2021). DNA affinity purification sequencing and transcriptional profiling reveal new aspects of nitrogen regulation in a filamentous fungus. Proc. Natl. Acad. Sci. USA *118*. e2009501118.
22. Turnbull, M.H., Goodall, R., and Stewart, G.R. (1995). The impact of mycorrhizal colonization upon nitrogen source utilization and metabolism in seedlings of *Eucalyptus grandis* Hill ex Maiden and *Eucalyptus maculata* Hook. Plant Cell Environ. *18*, 1386–1394.
23. Sangtiean, T., and Schmidt, S. (2002). Growth of subtropical ECM fungi with different nitrogen sources using a new floating culture technique. Mycol. Res. *106*, 74–85.
24. Guidot, A., Verner, M.C., Debaud, J.C., and Marmeisse, R. (2005). Intraspecific variation in use of different organic nitrogen sources by the ectomycorrhizal fungus *Hebeloma cylindrosporum*. Mycorrhiza *15*, 167–177.
25. Gallart, M., Adair, K.L., Love, J., Meason, D.F., Clinton, P.W., Xue, J., and Turnbull, M.H. (2018). Host genotype and nitrogen form shape the root microbiome of Pinus radiata. Microb. Ecol. *75*, 419–433.
26. Lin, Z., Wang, J., Bao, Y., Guo, Q., Powell, C.A., Xu, S., Chen, B., and Zhang, M. (2016). Deciphering the transcriptomic response of *Fusarium verticillioides* in relation to nitrogen availability and the development of sugarcane pokkah boeng disease. Sci. Rep. *6*, 29692.
27. Kaldorf, M., Koch, B., Rexer, K.H., Kost, G., and Varma, A. (2005). Patterns of interaction between *Populus* Esch5 and *Piriformospora indica*: a transition from mutualism to antagonism. Plant Biol. *7*, 210–218.
28. Newsham, K.K. (2011). A meta-analysis of plant responses to dark septate root endophytes. New Phytol. *190*, 783–793.
29. Qin, Y., Pan, X., Kubicek, C., Druzhinina, I., Chenthamara, K., Labbé, J., and Yuan, Z. (2017). Diverse plant-associated pleosporalean fungi from saline areas: ecological tolerance and nitrogen-status dependent effects on plant growth. Front. Microbiol. *8*, 158.
30. Quispe, C.F., Sonderman, O., Khasin, M., Riekhof, W.R., Van Etten, J.L., and Nickerson, K.W. (2016). Comparative genomics, transcriptomics, and physiology distinguish symbiotic from free-living *Chlorella* strains. Algal Res. *18*, 332–340.
31. Orton, P.D. (1960). New check list of British agarics and boleti: Part III. Trans. Br. Mycol. Soc. *43*, 159–384.
32. Baroni, T.J., and Halling, R.E. (2000). Some Entolomataceae (Agaricales) from Costa Rica. Brittonia *52*, 121–135.
33. Jin, W., Peng, L., Zhang, X., Sun, H., and Yuan, Z. (2019). Effects of endophytic and ectomycorrhizal basidiomycetes on *Quercus virginiana* plantlet growth and nutrient absorption. J. Sustain. For. *38*, 1–17.
34. Jin, W., Wang, Y., Sun, H., and Yuan, Z. (2021). A survey of the potential ectomycorrhizal fungi associated with nursery seedlings of seven species of exotic *Quercus* in China. J. Sustain. For. *40*, 357–370.
35. Peng, L., Shan, X., Yang, Y., Wang, Y., Druzhinina, I.S., Pan, X., Jin, W., He, X., Wang, X., Zhang, X., et al. (2021). Facultative symbiosis with a saprotrophic soil fungus promotes potassium uptake in American sweetgum trees. Plant Cell Environ. *44*, 2793–2809.
36. Torres, M.A., and Dangl, J.L. (2005). Functions of the respiratory burst oxidase in biotic interactions, abiotic stress and development. Curr. Opin. Plant Biol. *8*, 397–403.
37. Bhatt, M., Mistri, P., Joshi, I., Ram, H., Raval, R., Thoota, S., Patel, A., Raval, D., Bhargava, P., Soni, S., et al. (2018). Molecular survey of basidiomycetes and divergence time estimation: an Indian perspective. PLoS One *13*, e0197306.
38. Harmaja, H. (2003). Notes on *Clitocybe* s. lato (Agaricales). Ann. Bot. Fenn. *40*, 213–218.

39. Matheny, P.B., Curtis, J.M., Hofstetter, V., Aime, M.C., Moncalvo, J.M., Ge, Z.W., Slot, J.C., Ammirati, J.F., Baroni, T.J., Bougher, N.L., et al. (2006). Major clades of Agaricales: a multilocus phylogenetic overview. Mycologia *98*, 982–995.

40. Dentinger, B.T.M., Gaya, E., O'Brien, H., Suz, L.M., Lachlan, R., Díaz-Valderrama, J.R., Koch, R.A., and Aime, M.C. (2016). Tales from the crypt: genome mining from fungarium specimens improves resolution of the mushroom tree of life. Biol. J. Linn. Soc. *117*, 11–32.

41. Mello, A., and Balestrini, R. (2018). Recent insights on biological and ecological aspects of ectomycorrhizal fungi and their interactions. Front. Microbiol. *9*, 216.

42. Veneault-Fourrey, C., Commun, C., Kohler, A., Morin, E., Balestrini, R., Plett, J., Danchin, E., Coutinho, P., Wiebenga, A., de Vries, R.P., et al. (2014). Genomic and transcriptomic analysis of *Laccaria bicolor* CAZome reveals insights into polysaccharides remodelling during symbiosis establishment. Fungal Genet. Biol. *72*, 168–181.

43. Zhang, F., Anasontzis, G.E., Labourel, A., Champion, C., Haon, M., Kemppainen, M., Commun, C., Deveau, A., Pardo, A., Veneault-Fourrey, C., et al. (2018). The ectomycorrhizal basidiomycete *Laccaria bicolor* releases a secreted β-1,4 endoglucanase that plays a key role in symbiosis development. New Phytol. *220*, 1309–1321.

44. Zhang, F., Labourel, A., Haon, M., Kemppainen, M., Da Silva Machado, E., Brouilly, N., Veneault-Fourrey, C., Kohler, A., Rosso, M.N., Pardo, A., et al. (2022). The ectomycorrhizal basidiomycete *Laccaria bicolor* releases a GH28 polygalacturonase that plays a key role in symbiosis establishment. New Phytol. *233*, 2534–2547.

45. Peng, L., Shan, X., Wang, Y., Martin, F., Vilgalys, R., and Yuan, Z. (2021). Hybrid genome assembly and gene repertoire of the root endophyte *Clitopilus hobsonii* QYL-10 (Entolomataceae, Agaricales, Basidiomycetes). Mol. Plant Microbe Interact. *34*, 711–714.

46. Zuccaro, A., Lahrmann, U., Güldener, U., Langen, G., Pfiffi, S., Biedenkopf, D., Wong, P., Samans, B., Grimm, C., Basiewicz, M., et al. (2011). Endophytic life strategies decoded by genome and transcriptome analyses of the mutualistic root symbiont *Piriformospora indica*. PLoS Pathog. *7*, e1002290.

47. Sipos, G., Prasanna, A.N., Walter, M.C., O'Connor, E., Bálint, B., Krizsán, K., Kiss, B., Hess, J., Varga, T., Slot, J., et al. (2017). Genome expansion and lineage-specific genetic innovations in the forest pathogenic fungi *Armillaria*. Nat. Ecol. Evol. *1*, 1931–1941.

48. Martin, F., Aerts, A., Ahrén, D., Brun, A., Danchin, E.G., Duchaussoy, F., Gibon, J., Kohler, A., Lindquist, E., Pereda, V., et al. (2008). The genome of *Laccaria bicolor* provides insights into mycorrhizal symbiosis. Nature *452*, 88–92.

49. Chalot, M., and Brun, A. (1998). Physiology of organic nitrogen acquisition by ectomycorrhizal fungi and ectomycorrhizas. FEMS Microbiol. Rev. *22*, 21–44.

50. Spanu, P.D. (2012). The genomics of obligate (and nonobligate) biotrophs. Annu. Rev. Phytopathol. *50*, 91–109.

51. Snoeijers, S.S., Pérez-García, A., Joosten, M.H.A.J., and De Wit, P.J.G.M. (2000). The effect of nitrogen on disease development and gene expression in bacterial and fungal plant pathogens. Eur. J. Plant Pathol. *106*, 493–506.

52. Weng, Q., Zhang, X., Chen, W., and Hu, Q. (2019). Secondary metabolites and the risks of *Isaria fumosorosea* and *Isaria farinosa*. Molecules *24*, 664.

53. Venkatesh, N., and Keller, N.P. (2019). Mycotoxins in conversation with bacteria and fungi. Front. Microbiol. *10*, 403.

54. Ellström, M., Shah, F., Johansson, T., Ahrén, D., Persson, P., and Tunlid, A. (2015). The carbon starvation response of the ectomycorrhizal fungus *Paxillus involutus*. FEMS Microbiol. Ecol. *91*, fiv027.

55. Ray, P., Abraham, P.E., Guo, Y., Giannone, R.J., Engle, N.L., Yang, Z.K., Jacobson, D., Hettich, R.L., Tschaplinski, T.J., and Craven, K.D. (2019). Scavenging organic nitrogen and remodelling lipid metabolism are key survival strategies adopted by the endophytic fungi, *Serendipita vermifera* and *Serendipita bescii* to alleviate nitrogen and phosphorous starvation *in vitro*. Environmental Microbiology Reports *11*, 548–557.

56. Smith, J.M., Whiteside, M.D., and Jones, M.D. (2020). Rapid nitrogen loss from ectomycorrhizal pine germinants signaled by their fungal symbiont. Mycorrhiza *30*, 407–417.

57. Kohler, A., Kuo, A., Nagy, L.G., Morin, E., Barry, K.W., Buscot, F., Canbäck, B., Choi, C., Cichocki, N., Clum, A., et al. (2015). Convergent losses of decay mechanisms and rapid turnover of symbiosis genes in mycorrhizal mutualists. Nat. Genet. *47*, 410–415.

58. Miyauchi, S., Kiss, E., Kuo, A., Drula, E., Kohler, A., Sánchez-García, M., Morin, E., Andreopoulos, B., Barry, K.W., Bonito, G., et al. (2020). Large-scale genome sequencing of mycorrhizal fungi provides insights into the early evolution of symbiotic traits. Nat. Commun. *11*, 5125.

59. Selosse, M.A., Schneider-Maunoury, L., and Martos, F. (2018). Time to rethink fungal ecology? Fungal ecological niches are often prejudged. New Phytol. *217*, 968–972.

60. Mesny, F., Miyauchi, S., Thiergart, T., Pickel, B., Atanasova, L., Karlsson, M., Hüttel, B., Barry, K.W., Haridas, S., Chen, C., et al. (2021). Genetic determinants of endophytism in the Arabidopsis root mycobiome. Nat. Commun. *12*, 7227.

61. Zamioudis, C., and Pieterse, C.M. (2012). Modulation of host immunity by beneficial microbes. Mol. Plant Microbe Interact. *25*, 139–150.

62. Johnson, J.M., and Oelmüller, R. (2009). Mutualism or parasitism: life in an unstable continuum. What can we learn from the mutualistic interaction between Piriformospora indica and Arabidopsis thaliana? Endocytobiosis Cell Res. *19*, 81–110.

63. Sillo, F., Fangel, J.U., Henrissat, B., Faccio, A., Bonfante, P., Martin, F., Willats, W.G., and Balestrini, R. (2016). Understanding plant cell-wall remodelling during the symbiotic interaction between *Tuber melanosporum* and *Corylus avellana* using a carbohydrate microarray. Planta *244*, 347–359.

64. Martino, E., Morin, E., Grelet, G.A., Kuo, A., Kohler, A., Daghino, S., Barry, K.W., Cichocki, N., Clum, A., Dockter, R.B., et al. (2018). Comparative genomics and transcriptomics depict ericoid mycorrhizal fungi as versatile saprotrophs and plant mutualists. New Phytol. *217*, 1213–1229.

65. Hong, J.L., Wu, L., Lu, J.Q., Zhou, W.B., Cao, Y.J., Lv, W.L., Liu, B., Rao, P.F., Ni, L., and Lv, X.C. (2020). Comparative transcriptomic analysis reveals the regulatory effects of mineral nitrogen on the biosynthesis of *Monascus* pigments and citrinin. RSC Adv. *10*, 5268–5282.

66. Fochi, V., Chitarra, W., Kohler, A., Voyron, S., Singan, V.R., Lindquist, E.A., Barry, K.W., Girlanda, M., Grigoriev, I.V., Martin, F., et al. (2017). Fungal and plant gene expression in the *Tulasnella calospora–Serapias vomeracea* symbiosis provides clues about nitrogen pathways in orchid mycorrhizas. New Phytol. *213*, 365–379.

67. Scherm, B., Balmas, V., Spanu, F., Pani, G., Delogu, G., Pasquali, M., and Migheli, Q. (2013). *Fusarium culmorum*: causal agent of foot and root rot and head blight on wheat. Mol. Plant Pathol. *14*, 323–341.

68. Qiu, D., Xu, L., Vandemark, G., and Chen, W. (2016). Comparative transcriptome analysis between the fungal plant pathogens *Sclerotinia sclerotiorum* and *S. trifoliorum* using RNA sequencing. J. Hered. *107*, 163–172.

69. Doré, J., Kohler, A., Dubost, A., Hundley, H., Singan, V., Peng, Y., Kuo, A., Grigoriev, I.V., Martin, F., Marmeisse, R., and Gay, G. (2017). The ectomycorrhizal basidiomycete *Hebeloma cylindrosporum* undergoes early waves of transcriptional reprogramming prior to symbiotic structures differentiation. Environ. Microbiol. *19*, 1338–1354.

70. Brunner, P.C., Torriani, S.F., Croll, D., Stukenbrock, E.H., and McDonald, B.A. (2013). Coevolution and life cycle specialization of plant cell wall degrading enzymes in a hemibiotrophic pathogen. Mol. Biol. Evol. *30*, 1337–1347.

71. Druzhinina, I.S., Chenthamara, K., Zhang, J., Atanasova, L., Yang, D., Miao, Y., Rahimi, M.J., Grujic, M., Cai, F., Pourmehdi, S., et al. (2018). Massive lateral transfer of genes encoding plant cell wall-degrading enzymes to the mycoparasitic fungus *Trichoderma* from its plant-associated hosts. PLoS Genet. *14*, e1007322.

72. Li, P., Cai, Q., Wang, H., Li, S., Cheng, J., Li, H., Yu, Q., and Wu, S. (2020). Hydrogen peroxide homeostasis provides beneficial micro-environment for SHR-mediated periclinal division in Arabidopsis root. New Phytol. *228*, 1926–1938.

73. Emms, D.M., and Kelly, S. (2019). OrthoFinder: phylogenetic orthology inference for comparative genomics. Genome Biol. *20*, 238.

74. Edgar, R.C. (2004). MUSCLE: multiple sequence alignment with high accuracy and high throughput. Nucleic Acids Res. *32*, 1792–1797.

75. Zhang, H., Yohe, T., Huang, L., Entwistle, S., Wu, P., Yang, Z., Busk, P.K., Xu, Y., and Yin, Y. (2018). dbCAN2: a meta server for automated carbohydrate-active enzyme annotation. Nucleic Acids Res. *46*, W95–W101.

76. Almagro Armenteros, J.J., Tsirigos, K.D., Sønderby, C.K., Petersen, T.N., Winther, O., Brunak, S., von Heijne, G., and Nielsen, H. (2019). SignalP 5.0 improves signal peptide predictions using deep neural networks. Nat. Biotechnol. *37*, 420–423.

77. Blin, K., Wolf, T., Chevrette, M.G., Lu, X., Schwalen, C.J., Kautsar, S.A., Suarez Duran, H.G., de Los Santos, E., Kim, H.U., Nave, M., et al. (2017). antiSMASH 4.0-improvements in chemistry prediction and gene cluster boundary identification. Nucleic Acids Res. *45*, W36–W41.

78. Martin, M. (2011). Cutadapt removes adapter sequences from high-throughput sequencing reads. EMBnet J. *17*, 10–12.

79. Kim, D., Langmead, B., and Salzberg, S.L. (2015). HISAT: a fast spliced aligner with low memory requirements. Nat. Methods *12*, 357–360.

80. Li, B., and Dewey, C.N. (2011). RSEM: accurate transcript quantification from RNA-seq data with or without a reference genome. BMC Bioinformatics *12*, 323.

81. Robinson, M.D., McCarthy, D.J., and Smyth, G.K. (2010). edgeR: a Bioconductor package for differential expression analysis of digital gene expression data. Bioinformatics *26*, 139–140.

82. Zhang, N., Yu, H., Yu, H., Cai, Y., Huang, L., Xu, C., Xiong, G., Meng, X., Wang, J., Chen, H., et al. (2018). A core regulatory pathway controlling rice tiller angle mediated by the *LAZY1*-dependent asymmetric distribution of auxin. Plant Cell *30*, 1461–1475.

83. Xie, C., Mao, X., Huang, J., Ding, Y., Wu, J., Dong, S., Kong, L., Gao, G., Li, C.Y., and Wei, L. (2011). KOBAS 2.0: a web server for annotation and identification of enriched pathways and diseases. Nucleic Acids Res. *39*, W316–W322.

84. Murashige, T., and Skoog, F. (1962). A revised medium for rapid growth and bio assays with tobacco tissue cultures. Physiol. Plant. *15*, 473–497.

85. Mandyam, K., and Jumpponen, A. (2005). Seeking the elusive function of the root-colonising dark septate endophyte. Stud. Mycol. *53*, 173–189.

86. Vives-Peris, V., de Ollas, C., Gómez-Cadenas, A., and Pérez-Clemente, R.M. (2020). Root exudates: from plant to rhizosphere and beyond. Plant Cell Rep. *39*, 3–17.

87. Liu, C., Li, K., Wang, M., Fan, E., Yang, C., Wang, J., Fu, P., Ge, X., Sederoff, H.W., Sederoff, R.R., et al. (2021). Qu-2, a robust poplar suspension cell line for molecular biology. J. For. Res. *32*, 733–740.

88. Prados Rosales, R.C., and Di Pietro, A. (2008). Vegetative hyphal fusion is not essential for plant infection by *Fusarium oxysporum*. Eukaryot. Cell *7*, 162–171.

89. Horneck, D., and Miller, R.O. (1998). Determination of total nitrogen in plant tissue. In Handbook of Reference Methods for Plant Analysis, Y. Kalra, ed. (Taylor & Francis), pp. 75–83.

90. Bowman, R.A. (1988). A rapid method to determine total phosphorus in soils. Soil Sci. Soc. Am. J. *52*, 1301–1304.

91. Ho, I. (1987). Comparison of eight *Pisolithus tinctorius* isolates for growth rate, enzyme activity, and phytohormone production. Can. J. For. Res. *17*, 31–35.

92. Pan, X., Welti, R., and Wang, X. (2010). Quantitative analysis of major plant hormones in crude plant extracts by high-performance liquid chromatography-mass spectrometry. Nat. Protoc. *5*, 986–992.

93. Thoen, E., Harder, C.B., Kauserud, H., Botnen, S.S., Vik, U., Taylor, A.F.S., Menkis, A., and Skrede, I. (2020). *In vitro* evidence of root colonization suggests ecological versatility in the genus *Mycena*. New Phytol. *227*, 601–612.

94. Mochizuki, S., Saitoh, K.I., Minami, E., and Nishizawa, Y. (2011). Localization of probe-accessible chitin and characterization of genes encoding chitin-binding domains during rice–*Magnaporthe oryzae* interactions. J. Gen. Plant Pathol. *77*, 163–173.

95. Phillips, J.M., and Hayman, D.S. (1970). Improved procedures for clearing roots and staining parasitic and vesicular-arbuscular mycorrhizal fungi for rapid assessment of infection. Trans. Br. Mycol. Soc. *55*, 158–IN18.

96. Qi, J., Wang, J., Gong, Z., and Zhou, J.M. (2017). Apoplastic ROS signaling in plant immunity. Curr. Opin. Plant Biol. *38*, 92–100.

97. Fester, T., and Hause, G. (2005). Accumulation of reactive oxygen species in arbuscular mycorrhizal roots. Mycorrhiza *15*, 373–379.

98. Castresana, J. (2000). Selection of conserved blocks from multiple alignments for their use in phylogenetic analysis. Mol. Biol. Evol. *17*, 540–552.

99. Ruiz-Dueñas, F.J., Barrasa, J.M., Sánchez-García, M., Camarero, S., Miyauchi, S., Serrano, A., Linde, D., Babiker, R., Drula, E., Ayuso-Fernández, I., et al. (2021). Genomic analysis enlightens Agaricales lifestyle evolution and increasing peroxidase diversity. Mol. Biol. Evol. *38*, 1428–1446.

STAR★METHODS

KEY RESOURCES TABLE

REAGENT or RESOURCE	SOURCE	IDENTIFIER
Biological samples		
Populus tomentosa	Beijing Forestry University, China	N/A
Clitopilus hobsonii QYL-10 isolated from ECM root tips of *Quercus lyrata*	Jin et al.[33,34]	CGMCC 20208
Chemicals, peptides, and recombinant proteins		
Sucrose	Xilong scientific	CAT# 57-50-1
Indole-3-butyric acid (IBA)	Sigma-Aldrich	CAT# 133-32-4
Glutamine	Sangon Biotech	CAT# 56-85-9
Glycine	Sangon Biotech	CAT# 56-40-6
Valine	Sangon Biotech	CAT# 72-18-4
Leucine	Sangon Biotech	CAT# 61-90-5
Phenylalanine	Sangon Biotech	CAT# 61-91-2
Ammonium chloride	Sinopharm Chemical Reagent	CAT# 12125-02-9
Calcium nitrate	Sinopharm Chemical Reagent	CAT# 10124-37-5
Glucose	Sinopharm Chemical Reagent	CAT# 50-99-7
Monopotassium phosphate	Sinopharm Chemical Reagent	CAT# 778-77-0
Magnesium sulfate.H_2O	Sinopharm Chemical Reagent	CAT# 14168-73-1
Calcium chloride	Sinopharm Chemical Reagent	CAT# 10043-52-4
Sodium chloride	Sinopharm Chemical Reagent	CAT# 7647-14-5
Zinc sulfate	Sinopharm Chemical Reagent	CAT# 7733-02-0
EDTA - Iron III sodium salt	Sinopharm Chemical Reagent	CAT# 15708-41-5
Thiamine	Sangon Biotech	CAT# 67-03-8
Hydrochloric acid	Sinopharm Chemical Reagent	CAT# 7647-01-0
Bacto Agar	Difco Laboratories	Lot: 3220297
Sulfuric acid	Sinopharm Chemical Reagent	CAT# 7664-93-9
^{15}N-glycine	Macklin	CAT# 7299-33-4
Tissue OCT-Freeze Medium	Sakura Finetek,	Lot: 1035-00
Wheat Germ Agglutinin- Alexa Fluor 488 conjugate	Thermo Fisher	Lot: 2155276
Propidium iodide	Sigma-Aldrich	CAT# 25535-16-4
Tween 20	Sinopharm Chemical Reagent	CAT# 9005-64-5
Dipotassium phosphate	Sinopharm Chemical Reagent	CAT# 7758-11-4
Potassium hydroxide	Sinopharm Chemical Reagent	CAT# 1310-58-3
Lactic acid	Sinopharm Chemical Reagent	CAT# 50-21-5
Trypan blue	Sangon Biotech	CAT# 72-57-1
Glycerol	Sinopharm Chemical Reagent	CAT# 56-81-5
3, 3'-diaminobenzidine	Sigma-Aldrich	CAT# 868272-85-9
TRIzol Reagent	Invitrogen, CA, USA	CAT# 15596026
Deposited data		
Assembled genome of *Clitopilus hobsonii* QYL-10	NCBI	JADPMO000000000
Raw reads of transcriptome of *C. hobsonii* (free-living mycelia) under NH_4^+ condition-repeat 1	This work	NCBI: SRR13089187
Raw reads of transcriptome of *C. hobsonii* (free-living mycelia) under NH_4^+ condition-repeat 2	This work	NCBI: SRR13089186
Raw reads of transcriptome of *C. hobsonii* (free-living mycelia) under NH_4^+ condition-repeat 3	This work	NCBI: SRR13089185
Raw reads of transcriptome of *C. hobsonii* (free-living mycelia) under NO_3^- condition-repeat 1	This work	NCBI: SRR13089184

(*Continued on next page*)

Continued

REAGENT or RESOURCE	SOURCE	IDENTIFIER
Raw reads of transcriptome of *C. hobsonii* (free-living mycelia) under NO_3^- condition-repeat 2	This work	NCBI: SRR13089183
Raw reads of transcriptome of *C. hobsonii* (free-living mycelia) under NO_3^- condition-repeat 3	This work	NCBI: SRR13089182
Raw reads of transcriptome of *C. hobsonii* (free-living mycelia) under organic N condition-repeat 1	This work	NCBI: SRR13089181
Raw reads of transcriptome of *C. hobsonii* (free-living mycelia) under organic N condition-repeat 2	This work	NCBI: SRR13089180
Raw reads of transcriptome of *C. hobsonii* (free-living mycelia) under organic N condition-repeat 3	This work	NCBI: SRR13089179
Raw reads of transcriptome of *C. hobsonii* (in plant) under NH_4^+ condition-repeat 1	This work	NCBI: SRR17930468
Raw reads of transcriptome of *C. hobsonii* (in plant) under NH_4^+ condition-repeat 2	This work	NCBI: SRR17930467
Raw reads of transcriptome of *C. hobsonii* (in litter) under NH_4^+ condition-repeat 2	This work	NCBI: SRR17930466
Raw reads of transcriptome of *C. hobsonii* (in litter) under NH_4^+ condition-repeat 3	This work	NCBI: SRR17930465
Raw reads of transcriptome of *C. hobsonii* (in plant) under NH_4^+ condition-repeat 3	This work	NCBI: SRR17930464
Raw reads of transcriptome of *C. hobsonii* (in plant) under NO_3^- condition-repeat 1	This work	NCBI: SRR17930463
Raw reads of transcriptome of *C. hobsonii* (in plant) under NO_3^- condition-repeat 2	This work	NCBI: SRR17930462
Raw reads of transcriptome of *C. hobsonii* (in plant) under NO_3^- condition-repeat 3	This work	NCBI: SRR17930461
Raw reads of transcriptome of *C. hobsonii* (in plant) under organic N condition-repeat 1	This work	NCBI: SRR17930460
Raw reads of transcriptome of *C. hobsonii* (in plant) under organic N condition-repeat 2	This work	NCBI: SRR17930459
Raw reads of transcriptome of *C. hobsonii* (in plant) under organic N condition-repeat 3	This work	NCBI: SRR17930458
Raw reads of transcriptome of *C. hobsonii* (in litter) under NH_4^+ condition-repeat 1	This work	NCBI: SRR17930457
Experimental models: Cell lines		
Poplar suspension cell line Qu-2	Prof. Guanzhen Qu, Northeast Forestry University, China	N/A
Experimental models: Organisms/strains		
Tricholoma matsutake	JGI	https://mycocosm.jgi.doe.gov/Trima3/Trima3.home.html
Laccaria bicolor	JGI	https://mycocosm.jgi.doe.gov/Lacbi2/Lacbi2.home.html
Laccaria amethystina	JGI	https://mycocosm.jgi.doe.gov/Lacam2/Lacam2.home.html
Clitocybe gibba	JGI	https://mycocosm.jgi.doe.gov/Cligib1/Cligib1.home.html
Hypsizygus marmoreus	JGI	https://mycocosm.jgi.doe.gov/Hypma1/Hypma1.home.html
Lepista nuda	JGI	https://mycocosm.jgi.doe.gov/Lepnud1/Lepnud1.home.html
Hebeloma cylindrosporum	JGI	https://mycocosm.jgi.doe.gov/Hebcy2/Hebcy2.home.html

(*Continued on next page*)

Continued

REAGENT or RESOURCE	SOURCE	IDENTIFIER
Volvariella volvacea	JGI	https://mycocosm.jgi.doe.gov/Volvo1/Volvo1.home.html
Serendipita indica	JGI	https://mycocosm.jgi.doe.gov/Pirin1/Pirin1.home.html
Agaricus bisporus	JGI	https://mycocosm.jgi.doe.gov/Agabi_varbisH97_2/Agabi_varbisH97_2.home.html
Mycena galopus	JGI	https://mycocosm.jgi.doe.gov/Mycgal1/Mycgal1.home.html
Serpula himantioides	JGI	https://mycocosm.jgi.doe.gov/Serla_varsha1/Serla_varsha1.home.html
Coniophora puteana	JGI	https://mycocosm.jgi.doe.gov/Conpu1/Conpu1.home.html
Dacryopinax primogenitus	JGI	https://mycocosm.jgi.doe.gov/Dacsp1/Dacsp1.home.html
Fomitopsis pinicola	JGI	https://mycocosm.jgi.doe.gov/Fompi3/Fompi3.home.html
Gloeophyllum trabeum	JGI	https://mycocosm.jgi.doe.gov/Glotr1_1/Glotr1_1.home.html
Hydnomerulius pinastri	JGI	https://mycocosm.jgi.doe.gov/Hydpi2/Hydpi2.home.html
Software and algorithms		
ImageJ	Li et al.[72]	https://imagej.nih.gov/ij/
OrthoFinder v2.3.8	Emms and Kelly[73]	https://github.com/davidemms/OrthoFinder
MUSCLE v3.8.31	Edgar[74]	http://www.drive5. com/muscle
MrBayes v3.1.2	N/A	https://nbisweden.github.io/MrBayes/manual.html
PAML v4.9	N/A	http://abacus.gene.ucl.ac.uk/software/paml.html
dbCAN2 web-based meta server	Zhang et al.[75]	http://cys.bios.niu.edu/dbCAN2
Signal P	Almagro Armenteros et al.[76]	http://www.cbs.dtu.dk/services/SignalP/
antiSMASH v 4.0.2	Blin et al.[77]	http://antismash.secondarymetabolites.org
Cutadapt v1.9	Martin[78]	https://cutadapt.readthedocs.io/en/stable
HISAT2 v2.0.4	Kim et al.[79]	https://daehwankimlab.github.io/hisat2
StringTie v1.3.6	N/A	http://ccb.jhu.edu/software/stringtie
RSEM v1.3.0	Li and Dewey[80]	http://deweylab.biostat.wisc.edu/rsem
EdgeR v3.12.0	Robinson et al.[81]	http://bioconductor.org
R version 3.0	Zhang et al.[82]	https://www.r-project.org/
KOBAS	Xie et al.[83]	http://kobas.cbi.pku.edu.cn/home.do
IBM SPSS Statistics 20	IBM SPSS	http://www.spss.com.cn

RESOURCE AVAILABILITY

Lead contact

Further information and requests for resources and reagents should be directed to and will be fulfilled by the lead contact: Zhilin Yuan (yuanzl@caf.ac.cn)

Materials availability

This study did not generate any new unique reagents or materials to report.

Data and code availability

Raw reads of transcriptome were submitted to the NCBI SRA database under accession numbers SRR17930457, SRR17930458, SRR17930459, SRR17930460, SRR17930461, SRR17930462, SRR17930463, SRR17930464, SRR17930465, SRR17930466, SRR17930467, SRR17930468, SRR13089187, SRR13089186, SRR13089185, SRR13089184, SRR13089183, SRR13089182,

SRR13089181, SRR13089180, and SRR13089179. Genomic and transcriptomic sequencing data generated in this study are available at the National Center for Biotechnology Information under BioProjects PRJNA675211 and BioSample SAMN16692392. Accession numbers for the assembled genomes are JADPMO000000000.

Any additional information required to reanalyze the data reported in this paper is available from the lead contact upon request.

EXPERIMENTAL MODEL AND SUBJECT DETAILS

Gnotobiotic poplar cuttings and fungal culture conditions

Experiments were performed with clones of *P. tomentosa* cuttings. In detail, virus-free plants were propagated by micro-cuttings and cultured on half-strength Murashige and Skoog (MS) medium[84] with 2% (w/v) sucrose, and 0.1 mg l^{-1} indole-3-butyric acid (IBA) at 26 °C using a 10 h 12,000-lux light/14 h dark cycle in a growth chamber for rooting. After 3-4 weeks, uniform cuttings with well-developed roots were selected to carry out the inoculation experiments. The strain QYL-10 of *C. hobsonii* was isolated from ECM root tips of *Quercus lyrata*[33,34] and identified by Peng et al.[45] The ex-type living culture CGMCC 20208 was deposited in the China General Microbiological Culture Collection Center. The isolate was kept as mycelial suspensions in 20% (v/v) glycerol at -80 °C until its use. The colonies were grown on potato dextrose agar (PDA) medium for one week at 24 °C.

In vitro fungal growth under three N forms

To assess the effect of N forms on the fungal growth and physiology, NH_4Cl, Ca $(NO_3)_2$, and a mixture of acidic, neutral, and aromatic amino acids [(glutamine (Glu), glycine (Gly), valine (Val), leucine (Leu), and phenylalanine (Phe)] (organic N) were separately added into base medium with a final concentration of 3.57 mM for all N forms. We used amino acid mixtures as they constitute a major reserve of soil organic N.[85] The base medium contained (l^{-1}): 2.0 g glucose, 0.30 g KH_2PO_4, 0.14 g $MgSO_4 \cdot H_2O$, 50 mg $CaCl_2$, 25 mg NaCl, 3 mg $ZnSO_4$, 12.5 mg ferric EDTA and 0.13 mg thiamine HCl, pH 5.8 prior to autoclaving. The organic N solutions were filter-sterilized with 0.22 μm Millipore filters and added into the autoclaved N-free basal medium.[29] The solid medium was prepared with 6.0 g l^{-1} Bacto Agar (Difco Laboratories, MI, USA). The colony diameter was measured every 2 days for 12 days. The measurement was performed for at least five replicates per condition.

Fungal liquid cultures were initiated by inoculating 10 one-week-old mycelial plugs (5 mm-diameter) to 100 ml of the liquid medium with different N sources. After 4 weeks stationary incubation in the dark at 24 °C, the mycelia were filtered, then oven-drying at 65 °C to constant weight. The initial and final pH value of liquid medium were measured by SevenCompact pH meter (Mettler Toledo, Zurich, Switzerland) (Figure S1).

METHOD DETAILS

Experimental design of dual interactions under three N forms

Three experimental designs were utilized during this work. First, plant–fungus co-cultures were constructed on solid medium with different N forms. Two 5-mm diameter mycelial plugs of actively growing fungus were placed on medium in sterile glass culture containers 650 ml in volume, 22 cm in height, and 9 cm in diameter. Controls consisted of mock inoculated sterile PDA plugs. Uniformly sized cuttings were transplanted into another container after one week (two plants per container) in contact with the mycelium. The main purpose of pre-inoculating the media with *C. hobsonii* was to avoid the potential effects of root exudates on modifying fungal metabolism.[86] These microcosms were kept in growth chambers at 26 °C using a 10 h 12,000-lux light/14 h dark cycle. Three replicates of each treatment group were set up (four plants per replicate). Plant growth and different nutrient concentrations were measured after 4 weeks of incubation. Additionally, a small portion of the colonized roots was used to observe fungal colonization patterns.

Second, detached living poplar leaves were used to assess whether changes in fungal metabolism, caused by different N forms, affected aboveground plant tissues. According to a method described by Kaldorf et al.,[27] two 5-mm diameter plugs were inoculated in Petri dishes containing media with different N forms. These cultures were incubated in the dark for one week. At this point, leaves from gnotobiotic poplar cuttings were cut and placed on the surface of fungal colonies. The leaves were covered with a sterile glass slide to guarantee tight contact with the fungus. Conditions during incubation were the same as described above. After one week incubation, leaves were photographed. At the end of the experiment (4 weeks of incubation), the morphological characteristics of the leaf margin, potential leaf lesions, and the cut ends of petioles were recorded by an ultra-depth-of-field optical microscope (Keyence, Osaka, Japan).

Third, we obtained crude extracts from liquid cultures of *C. hobsonii* to treat the poplar suspension cell line Qu-2 derived from a hybrid poplar (*P. alba* × *P. berolinensis*). The suspension cells were cultured using the method described by Liu et al.[87] Fungal liquid cultures were initiated from one-week-old PDA by inoculating ten mycelial plugs, 5 mm-diameter each, into 500 ml of liquid media supplemented with the three N forms as described above. Flasks were incubated at 26 °C in the dark, without shaking. After one month, the mycelia were harvested using filter paper. The culture filtrate and mycelial mats were separately extracted twice with acetone and ethyl acetate. Solvents were evaporated under vacuum on a rotary evaporator at 45 °C to yield residues. These were lyophilized to constant weight using a vacuum-freeze drier (Labconco, KS, USA). The residues were re-dissolved in sterile water, passed through a 0.22-μm Millipore filter, and quantified before addition to the cell culture at a final concentration of 50 mg ml^{-1}. Sterile water served as control. During these experiments 500 μl of extract solution was added to suspension cell cultures. The cells

were sampled every 2 days, and the number of cells per unit volume was counted using a hemocytometer. Each experiment was performed in triplicate.

Cellophane penetration test

To mimic the process occurring during the early stages of fungal colonization when hyphae penetrate root tissues, we compared the impact of N forms on fungal infection ability by using an *in vitro* penetration assay.[88] Autoclaved colorless cellophane sheets were placed on plates[88] containing the above-mentioned three N form-based media and the center of each plate was inoculated with a plug (5 mm-diameter). After 2 weeks at 24 °C in the dark, the cellophane sheet with the fungal colony was removed. The presence or absence of fungal mycelia on the underlying medium was recorded after incubation of the plates for an additional period of 2 days at 24 °C in the dark. All experiments included at least three biological replicates.

Plant phenotypic assay

Fresh roots and shoots were weighed. Total root length, root surface area, root volume, number of root tips, were determined using image analysis software (Regent Instruments, Quebec, Canada). Total N, P and K concentrations in above and belowground plant parts were quantified by the Kjeldahl digestion procedure,[89] Mo-Sb colorimetric method after digestion with H_2SO_4-H_2O_2[90] and ICP-AES system of iCAP 6300 (Thermo Fisher Scientific, CA, USA), respectively. All experiments included at least three biological replicates.

In vitro fungal phytohormone production

We used modified Melin-Norkrans (MMN) medium without malt extract and vitamin B1 for fungal culturing and phytohormone measurements.[91] The mycelium of *C. hobsonii* was grown at pH 5.8 and 24 °C for 3 weeks. We did not compare the phytohormone profiling of the fungus grown on the three N forms for two reasons due to the very poor growth of *C. hobsonii* on NO_3^-. First, our main purpose was to evaluate its potential to produce phytohormone *in vitro*. Second, the very poor growth of *C. hobsonii* under NO_3^- condition prevented us from obtaining adequate mycelial biomass for sample preparations. We quantified the concentrations of phytohormones from the mycelia and filtrates. The indole-3-acetic acid (IAA), IBA, abscisic acid (ABA), trans-zeatin-riboside (TZR), zeatin, jasmonic acid (JA), gibberellins (GA), salicylic acid (SA), methyl jasmonic acid (MeJA), and methyl salicylic acid (MeSA) were determined using reverse-phase liquid chromatography-tandem mass spectrometry (Thermo Scientific, MA, USA) with multiple reaction monitoring using a stable isotope labeled internal standard.[92] Three independent biological replicates were performed.

Isotopic tracing using ^{15}N glycine labelling

To assess whether *C. hobsonii* translocate N to the host plant, we conducted isotope tracer experiments. ^{15}N-glycine was selected as the isotopic label for organic N uptake because glycine was more readily utilized by *C. hobsonii* than Glu, Val, Leu, or Phe. Microcosms were constructed according to the method of Thoen et al.[93] A 90-mm split Petri dish was used to create a plant and a fungus compartment in each microcosm, with a barrier to prevent the leakage of the tracer between them. A 0.5-mm nylon mesh in the middle of these split Petri dishes acted as a barrier avoiding the growth of the plant roots into the fungal compartment. The split dish was filled with 23 ml of organic N medium. On the fungal side of the microcosm, a small 35-mm diameter Petri dish was inserted and filled with approximately 8.5 ml of organic N medium containing the ^{15}N-glycine (at 99 atom % ^{15}N excess). This small Petri dish acted as an additional barrier, preventing the leakage of the tracer into the surrounding agar. A 5-mm diameter mycelial plug was placed on one side of the split Petri dish. On the plant side a small hole was made, using a hot scalpel, to allow the shoot to grow outside of the dish. Sterile seedlings were added to the plant side of the microcosm, restricting roots to the plant side. Petri dishes, sealed with a double layer of Parafilm, were placed inside a bigger, 150 × 150-mm square Petri dish. A sterile, moistened cotton wool ball was inserted into this square Petri dish, to protect the seedlings from drying out. The entire system was sealed with a double layer of Parafilm and then covered in aluminum foil to keep the roots in the dark. Microcosms were maintained in a growth chamber for 4 weeks at 26 °C using a 10 h 12,000-lux light/14 h dark cycle. Some of the dishes, serving as controls, were not inoculated.

Given that shoots and leave tissues vary in isotopic composition, to ensure comparability the aboveground part of the plant was divided into half of each shoot and half of the leaves. Before isotopic analysis, plants were finely ground and dried at 65 °C to a constant weight, and then stored in scintillation vials. ^{15}N levels in shoots and roots were measured using an IsoPrime100 isotope ratio mass spectrometer (Isoprime, Cheadle Hulme, UK), following the manufacturer's instructions. Stable isotope data were reported as:

$$\delta^{15}N\ (‰) = (R_{sample} / R_{standard} - 1) \times 1000$$

where R was the corresponding $^{15}N/^{14}N$ ratio for either a given sample or the atmospheric N_2 standard used for ^{15}N isotopic fractionation. The analytical precision of the isotopic measurements in multiple replicate analyses was 0.2‰.

Semi-quantitative measurement of fungal enzymatic profiling

To measure enzymatic activities in fungal mycelia under different nitrogen form conditions, we employed API ZYM (BioMerieux, Madrid, Spain) system, following the manufacturer's instructions. The API ZYM strips consist of 20 microcupules containing dehydrated chromogenic substrates of 19 different enzymes and a control (a microcupule that does not contain any enzyme substrate). These enzymes include three phosphatases (alkaline phosphatase, acid phosphatase and phosphohydrolase), three esterases (lipase,

esterase–lipase and esterase), three aminopeptidases (leucine amino-peptidase, valine amino-peptidase and cystine amino- peptidase), two proteases (chymotrypsin and trypsin), and eight glycosyl-hydrolases (β-galactosidase, β-glucosidase, N-acetyl-β- glucosaminidase, α-glucosidase, α-galactosidase, β-glucuronidase, α-mannosidase and α-fucosidase). The fungal samples were ground under low temperatures. The enzyme extracts were prepared by mixing approximately 190 mg of fungal material powder from each treatment with 4 ml sterile water. After the enzyme extracts had been prepared, an aliquot (65 μL) of the extract supernate was dispensed into each of the 20 microcupules. The API ZYM strips were then covered and incubated at 37 °C for 4 h. After incubation, 30 μL of each reagent (ZYM A and ZYM B; BioMerieux) were added to all microcupules. After 5 min, a numerical value of 1-5 was assigned to each microcupule according to the colour chart provided by the manufacturer. For the purposes of this study, the results were reported as reactions of not detected (0), very low intensity (1), low intensity (2), moderate intensity (3), high intensity (4) and very high intensity (5) (Figure S4).

Confocal section and squash mounts for fungal visualization in roots

As the mineral N was detrimental to plant–fungus associations, we set out to visualize patterns of fungal colonization of the roots under organic N condition, in which the development of ECM-like structures appeared. A handful of well-developed ECM-like root tips 4 weeks post-inoculation were selected and fixed in 75% ethanol (v/v). The roots were then rinsed with 50 mM phosphate-buffered saline (PBS, pH 7.4) and embedded in Tissue OCT-Freeze Medium (Sakura Finetek, CA, USA). Transversal sections (8-10 μm in thickness) of root tips were prepared using a Thermo Cryostar NX70 freezing microtome (Thermo Fisher Scientific, Walldorf, Germany), and dual staining of the fungal cell wall (Wheat Germ Agglutinin- Alexa Fluor 488 conjugate, WGA-AF488) (Thermo Fisher Scientific, MA, USA) and the plant cell wall (Propidium iodide, PI) (Sigma-Aldrich, MO, USA) was carried out.[94] Samples were infiltrated with the staining solution (20 μg ml^{-1} PI, 20 μg ml^{-1} WGA, 0.1% Tween 20 made up in PBS) for 4 h. All the sections were viewed at 400 to 1000× magnification under a confocal laser scanning microscopy (Carl Zeiss, Jena, Germany) equipped with ZEN2 software. Mantle-like structures were only scored as present if layers of hyphae were present around all the examined root tip sections.

In addition, squash mounts were used as needed to observe potential infection structures in non-mycorrhizal roots. A subset of the harvested roots was fixed in 50% ethanol (v/v) and stained with trypan blue.[95] Roots were cleared with 5% KOH (w/v) at room temperature for one week, acidified in 2% lactic acid (v/v) for 1–2 min followed by strained with 0.05% (w/v) trypan blue (dissolved in a mixture of 1:1:1 lactic acid/glycerol/distilled water) for 3 h. The slides were photographed with a light microscope (Carl Zeiss, Jena, Germany) (Figure S3).

In situ detection of hydrogen peroxide production in roots upon colonization

Given that reactive oxygen species (ROS) play an integral role as signaling molecules in plant immune response triggered by a fungal infection,[96] we performed *in situ* detection of hydrogen peroxide (H_2O_2) in the roots. We used the 3, 3'-diaminobenzidine (DAB, Sigma-Aldrich, MO, USA) substrate as it efficiently reacts with H_2O_2 and forms reddish-brown polymer. Following the plant inoculation procedure mentioned above, root samples collected at 12, and 60 h after inoculation were collected and incubated in 1 mg ml^{-1} DAB in sodium citrate buffer at room temperature overnight, then washed and cleared with 10% (v/v) lactic acid.[97] Stained roots were imaged at a light microscope (Carl Zeiss, Jena, Germany) equipped *with* an AxioCam MRc5 digital camera. At least twelve root tips from each treatment were inspected. To quantify DAB staining results, the surface of brown areas of the DAB-H_2O_2 reaction were scored with ImageJ (https://imagej.nih.gov/ij/).[72]

Phylogenomic and comparative genomic analysis

Near-chromosome-level assembly of *C. hobsonii* was released,[45] and genomic data from 17 Agaricales species with saprotrophic or ECM lifestyles, which were referred to as close relatives of *C. hobsonii*, were downloaded from the JGI MycoCosm database. These data were used for phylogenetic reconstruction and comparative genomic analysis (http://jgi.doe.gov/fungi).[57,58] *S. indica* was used as an outgroup. We determined gene families or orthologous groups of these species by OrthoFinder v2.3.8 with the default inflation parameter of 1.5.[73] After filtering short low-quality genes (encoding proteins with < 200 amino acids), 1,654 single-copy gens were used for constructing a phylogenomic tree. The single-copy orthologous protein-coding sequences were aligned using MUSCLE v3.8.31.[74] The unambiguously aligned conserved blocks were extracted using Gblocks 0.91b with default parameters.[98] The concatenated alignment was used to create a Bayesian inference of phylogeny using MrBayes v3.1.2 (https://nbisweden.github.io/MrBayes/manual.html). Divergence time of each tree node was inferred using Bayesian Markov-chain Monte Carlo (MCMC) tree (MCMCTree) package in PAML v4.9 (http://abacus.gene.ucl.ac.uk/software/paml.html) with the GTR nucleotide substitution model. The phylogeny was calibrated using three calibration points as follows: *Laccaria amethystina–L. bicolor*, 17 Mya; *Lepista nuda–Tricholoma matsutake*, 96 Mya; *Clitocybe gibba*, 125 Mya.[99]

Our comparative analyses focused on gene categories involved in plant cell-wall degradation (PCWDEs), potential secondary metabolites (*e.g*, biosynthetic gene clusters (BGCs)), and N metabolism. All predicted carbohydrate-active enzymes (CAZyme) gene models were functionally annotated using the dbCAN2 web-based meta server (http://cys.bios.niu.edu/dbCAN2).[75] We focused on the secreted CAZyme repertoires, as they were released into the medium or the plant apoplastic space to degrade extracellular cellulose, pectin, lignin, and other polymers. To identify the secreted CAZymes, Signal P (http://www.cbs.dtu.dk/services/SignalP/)[76] a dedicated web program was used. The BGCs were predicted using antiSMASH v 4.0.2 (http://antismash.secondarymetabolites.org).[77]

Genome-wide fungal transcriptomic signatures *in vitro* and *in planta*

Transcriptomic analysis was performed for *C. hobsonii in vitro* (feeding on three N forms and autoclaved litters) and *in planta*. For *in vitro* assay, fungal colonies were grown on agar media containing three N sources (as described above) covered with cellophane membranes for 2 weeks at 24 °C. The mycelium grown on each plate was gently scraped from the cellophane, then mycelia were collected, snap frozen in liquid nitrogen, and stored at −80 °C until further analysis. The mixed poplar and oak leaf litters were sterilized by autoclaving at 121 °C for 30 min and transferred to the surface of sterile agar media. We harvested the samples until the litters were heavily colonized by *C. hobsonii* mycelium. For *in planta* assay, fungal transcripts were investigated in infected roots grown on three N conditions. After 12 days of co-cultivation, the colonized roots were used for RNA extractions. The total number of different expression genes (DEGs) found for each pairwise comparison between cultured mycelia across all six conditions and those cultured on litters (Table S1). Summary of RNA-seq data from 21 libraries was shown in Table S2. Transcripts with FPKM (the fragments per kilobase per million mapped reads) values equal to or greater than 5 in at least one sample were provided in Table S3.

RNA isolation and RNA-seq analyses

Total RNA was extracted using TRIzol Reagent (Invitrogen, CA, USA), according the manufacturer's instructions (Invitrogen). The RNA quality was determined by 2100 Bioanalyser (Agilent, CA, USA) and quantified using the ND-2000 (NanoDrop Technologies, Wilmington, DE, USA). The RNA was then reverse-transcribed to create the final cDNA library, by following the protocol of the mRNA-Seq sample preparation kit (Illumina, CA, USA). Paired-end RNA-seq sequencing library was sequenced with the Illumina HiSeq xten/NovaSeq 6000 sequencer (2 × 150 bp read length) at Shanghai Majorbio Bio-pharm Technology (Shanghai, China) (Illumina, CA, USA). For all RNA-seq experiments, three separate libraries were prepared from three biological replicates for each condition. A total of 21 individual cDNA libraries were constructed.

To get high quality clean reads, raw reads were further filtered by Cutadapt v1.9 (https://cutadapt.readthedocs.io/en/stable).[78] The clean reads were obtained from the 21 libraries, ranging from 40.05 to 52.60 million for each sample. We mapped these reads to the reference genome of *C. hobsonii* QYL-10 (http://www.ncbi.nlm.nih.gov/assembly/GCA_015708445.2) using HISAT2 v2.0.4 (https://daehwankimlab.github.io/hisat2) software.[79] HISAT2 allows multiple alignments per read (up to 20 by default) and a maximum of two mismatch when mapping the reads to the reference. StringTie v1.3.6 (http://ccb.jhu.edu/software/stringtie) was used to perform expression level for mRNAs by calculating FPKM (FPKM = [total exon fragments / mapped reads (millions) × exon length (kb)]). In our case, we used a minimum expression cut-off of 5 FPKM in order to exclude genes that are expressed at low levels without biological relevance. DEGs between each sample were identified on the basis of FPKM values and pairwise comparisons using RSEM v1.3.0 and EdgeR v3.12.0, with a false discovery rate (FDR) threshold of < 0.05 and $|\log FC| \geq 1$.[80,81] To identify more additionally important DEGs linked to lifestyle-related traits, we narrowed down the comparison to genes exhibiting the highest fold changes, some showing > 100-fold change in expression (Figure S7).

To determine whether there were transcriptionally distinct states for the fungus growing on three N sources, sub-clustering analysis was conducted. More specifically, we used log-transformed FPKM values to perform the hierarchical clustering algorithm with the hclust function in R version 3.0.[82] Pathway enrichment analysis based on gene count assigned in specific KEGG pathways for upregulated DEGs from organic N-fed mycelia were analyzed. The KEGG pathway analysis was performed by KOBAS (http://kobas.cbi.pku.edu.cn/home.do).[83]

QUANTIFICATION AND STATISTICAL ANALYSIS

The normality and variance homogeneity of all phenotypic and physiological data sets were evaluated by the Shapiro-Wilk's and Levene's tests, respectively. All data sets were subjected to different statistical tests depending on the type of data. Significant differences (plant biomass, root traits, nutrient element concentrations) between inoculated and un-inoculated trees grown on organic N condition were estimated with a Student's two-sample t-test at $P \leq 0.05$ using the IBM SPSS Statistics 20 software program (SPSS Inc., http://www.spss.com.cn). Significant differences (suspension cell diameter, numbers of suspension cell, DAB staining intensity, fungal colony diameter, and dry weight of mycelia) were estimated with a one-way analysis of variance (ANOVA) using IBM SPSS Statistics 20 software program (SPSS Inc., http://www.spss.com.cn). Each ANOVA was followed by the Tukey's *post hoc* test at $P \leq 0.05$. For comparison of averaged normalized expression values for each cluster of CAZyme genes, statistical significance was calculated using the Mann–Whitney U-test at $P \leq 0.05$, which assumes the measurements on a rank-order scale but does not assume normality of data. All data were expressed as mean values with standard deviations (SD).